HHS Public Access

Author manuscript

ACS Infect Dis. Author manuscript; available in PMC 2024 February 01.

Published in final edited form as:

ACS Infect Dis. 2021 June 11; 7(6): 1519–1534. doi:10.1021/acsinfecdis.1c00070.

Small-Molecule Inhibitors of the Coronavirus Spike – ACE2 Protein-Protein Interaction as Blockers of Viral Attachment and Entry for SARS-CoV-2

Damir Bojadzic[1], **Oscar Alcazar**[1], **Jinshui Chen**[1], **Sung-Ting Chuang**[1], **Jose M. Condor Capcha**[2,3], **Lina A. Shehadeh**[2,3,4], **Peter Buchwald**[*,1,5]

[1]Diabetes Research Institute, University of Miami, Miami, Florida, USA.

[2]Division of Cardiology, University of Miami, Miami, Florida, USA.

[3]Interdisciplinary Stem Cell Institute, University of Miami, Miami, Florida, USA.

[4]Peggy and Harold Katz Family Drug Discovery Center, University of Miami, Miami, Florida, USA.

[5]Department of Molecular and Cellular Pharmacology, Miller School of Medicine, University of Miami, Miami, Florida, USA.

Abstract

Inhibitors of the protein-protein interaction (PPI) between the SARS-CoV-2 spike protein and human ACE2 (hACE2), which acts as a ligand-receptor pair that initiates the viral attachment and cellular entry of this coronavirus causing the ongoing COVID-19 pandemic, are of considerable interest as potential antiviral agents. While blockade of such PPIs with small molecules is more challenging than with antibodies, small-molecule inhibitors (SMIs) might offer alternatives that are less strain- and mutation-sensitive, suitable for oral or inhaled administration, and more controllable / less immunogenic. Here, we report the identification of SMIs of this PPI by screening our compound-library focused around the chemical space of organic dyes. Among promising candidates identified, several dyes (Congo red, direct violet 1, Evans blue) and novel drug-like compounds (DRI-C23041, DRI-C91005) inhibited the interaction of hACE2 with the spike proteins of SARS-CoV-2 as well as SARS-CoV with low micromolar activity in our cell-free ELISA-type assays (IC_{50}s of 0.2-3.0 μM); whereas, control compounds, such as sunset yellow FCF, chloroquine, and suramin, showed no activity. Protein thermal shift assays indicated that the SMIs of interest identified here bind SARS-CoV-2-S and not hACE2. While

[*]Corresponding author: Phone: 305 243-9657, pbuchwald@med.miami.edu, Diabetes Research Institute, Miller School of Medicine, University of Miami, 1450 NW 10 Ave, Miami, FL 33136, USA.

AUTHOR CONTRIBUTIONS

DB performed the binding assays; DB and STC the thermal shift assays; OA, STC, and JMCC the pseudovirus assays; JC the chemical synthesis; LAS provided materials and analyzed the data. PB originated and designed the project, provided study guidance, analyzed the data, and wrote the draft manuscript. All authors contributed to writing and read the final manuscript.

CONFLICTS OF INTEREST

The University of Miami has filed a patent on these compounds and their use for this application with PB as inventor. All other authors declare that the research was conducted in the absence of any commercial or financial relationships that could be construed as a potential conflict of interest.

SUPPORTING INFORMATIONS

Supporting Information for this article is available at the end of this file and includes Supplementary Methods, Schemes S1 to S6, and Figures S1 to S3.

dyes seemed promiscuous inhibitors, DRI-C23041 showed some selectivity and inhibited the entry of two different SARS-CoV-2-S expressing pseudoviruses into hACE2-expressing cells in a concentration-dependent manner with low micromolar IC_{50}s (6-7 μM). This provides proof-of-principle evidence for the feasibility of small-molecule inhibition of PPIs critical for SARS-CoV-2 attachment/entry and serves as a first guide in the search for SMI-based alternative antiviral therapies for the prevention and treatment of diseases caused by coronaviruses in general and COVID-19 in particular.

Graphical Abstract

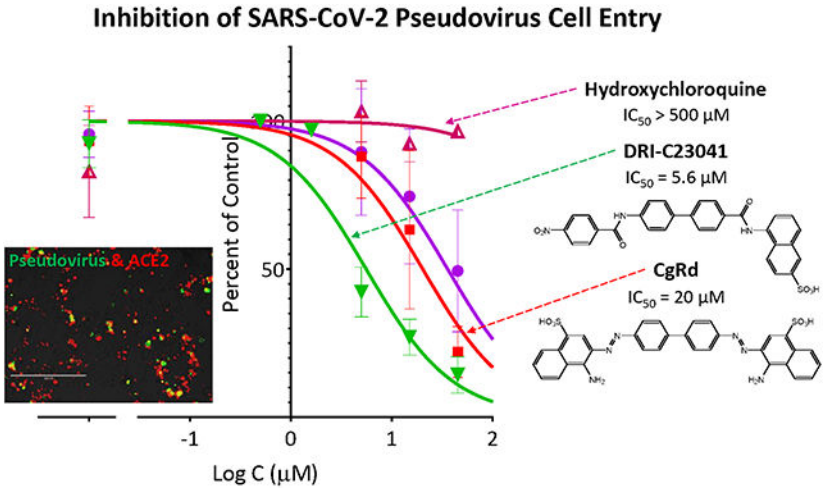

Keywords

ACE2; antiviral; coronavirus; protein-protein interaction; SARS-CoV-2; spike protein

COVID-19, which reached pandemic levels in early 2020 (WHO; March 11, 2020), is caused by the severe acute respiratory syndrome-coronavirus 2 (SARS-CoV-2) [1-3]. SARS-CoV-2 is the most infectious agent in a century [4], having already caused more than a hundred million infections and two million deaths worldwide. This coronavirus (CoV) is an enveloped, positive-sense RNA virus with a large RNA genome of roughly 29.9 kilobases and a diameter of up to about 120 nm, characterized by club-like spikes emerging from its surface [5, 6]. It is the most recently emerged among the seven CoVs known to infect humans. They include four CoVs that are responsible for about a third of the common cold cases (HCoV 229E, OC43, NL63, and HKU1) and three that caused epidemics in the last two decades associated with considerable mortality: SARS-CoV-1 (2002–2003, ~10% mortality), MERS-CoV (Middle East respiratory syndrome coronavirus; 2012, ~35% mortality), and now SARS-CoV-2 (2019–2020), which seems to be less lethal but more transmissible [7, 8]. While the SARS-CoV-2 situation is still evolving, current estimates indicate that about 3% of infected individuals need hospitalization and the average infection fatality ratio (IFR, percentage of those infected that do not survive) is around 0.5% but in a strongly age-dependent manner, i.e., increasing in log-linear manner from 0.001% in <20 years old to 8.3% in those >80 years old [9, 10] (to be compared with an IFR of <0.1% for

influenza). This created unprecedented health and economic damage and a correspondingly significant therapeutic need for possible preventive and/or curative treatments. As future CoVs that are highly contagious and/or lethal are also likely to emerge, novel therapies that could neutralize multiple strains are of particular interest especially as the large WHO Solidarity trial suggested that repurposed antiviral drugs including hydroxychloroquine, remdesivir, lopinavir, and interferon-β1, appear to have little or no effect on hospitalized COVID-19 patients, as indicated by overall mortality, initiation of ventilation, and duration of hospital stay [11].

Viral attachment and entry are of particular interest among possible therapeutic targets in the life cycle of viruses [7] because they represent the first steps in the replication cycle and take place at a relatively accessible extracellular site; they have indeed been explored for different viruses [12]. CoVs use the receptor-binding domain (RBD) of their glycosylated S protein to bind to cell specific surface receptors and initiate membrane fusion and virus entry. For both SARS-CoV and SARS-CoV-2, this involves binding to human angiotensin converting enzyme 2 (hACE2) followed by proteolytic activation by human proteases [3, 5, 13, 14]. Hence, blockade of the RBD–hACE2 protein-protein interaction (PPI) can disrupt infection efficiency, and most vaccines and neutralizing antibodies (nAbs) aim to abrogate this interaction [15, 16]. CoV nAbs, including those identified so far for SARS-CoV-2, primarily target the trimeric S glycoproteins, and their majority recognizes epitopes within the RBD that binds the ACE2 receptor [16-20]. It would be important to have broadly cross-reactive nAbs that can neutralize a wide range of viruses that share similar pathogenic outcomes [18]. The S proteins of SARS-CoV, MERS-CoV, and SARS-CoV-2 have similar structures with 1100–1300 amino acids and RBDs spanning about 200 residues and consisting of core and external subdomains, with the RBD cores being responsible for the formation of S trimers – similarities that allow the possibility of broad neutralization [21, 22]. SARS-CoV and SARS-CoV-2 share ~80% amino acid identity in their S proteins [16, 21]; nevertheless, most current evidence indicates that SARS-CoV antibodies are not cross-reactive for SARS-CoV-2 [23]. For example, one study found that none of the 206 RBD-specific monoclonal antibodies derived from single B cells of eight SARS-CoV-2 infected individuals cross-reacted with SARS-CoV or MERS-CoV RBDs [24]. Antibody-like monobodies designed to bound to the SARS-CoV-2 S protein also did not bind that of SARS-CoV [25]. As a further complicating factor, RNA viruses accumulate mutations over time, which yields antibody resistance and requires the use of antibody cocktails to avoid mutational escape [26]. Not surprisingly, there is now evidence of the emergence of SARS-CoV-2 mutants for which antibodies against the original strain have no or diminished activity [27].

In addition to being too highly target-specific, antibodies, as all protein therapies, are hindered by problems related to their solubility, unsuitability for oral or inhaled administration, and immunogenicity. By being foreign proteins, they themselves can act as antigens and elicit strong immune responses in certain patients [28-30], and this is only further exacerbated by their long elimination half-lives [31]. Even among FDA approved therapeutics, there were more post-market safety issues with biologics than with small-molecule drugs [32]. Hence, peptides or small molecules can offer alternative approaches. Some peptide disruptors of this PPI have also been reported, but so far none have been very effective [23, 33-35]. More importantly, because of bioavailability, metabolic instability

(short half-life), lack of membrane permeability, and other issues, developing peptides into clinically approved drugs is difficult and rarely pursued [36, 37].

Small molecules traditionally were not considered for PPI modulation because they were deemed unlikely to be successful due to the lack of well-defined binding pockets on the protein surface that would allow their adequate binding. During the last decade, however, it has become increasingly clear that SMIs can be effective against certain PPIs. There are now >40 PPIs targeted by SMIs that are in preclinical development [38-44], and two of them (venetoclax [45], lifitegrast [46]) were recently approved by the FDA for clinical use [47, 48]. Notably, the success of three small-molecule drugs that target HIV-1 entry and are now approved for clinical use, enfuvirtide, maraviroc, and fostemsavir validates this strategy of antiviral drug discovery. Maraviroc targets the C-C motif chemokine receptor 5 (CCR5), a host protein used as a co-receptor during HIV-1 entry, and it is a noncompetitive allosteric inhibitor that stabilizes a conformation no longer recognized by the viral envelope [12, 49]. Hence, it is an allosteric SMI of a PPI, highlighting the feasibility of such an approach to prevent viral entry. Interestingly, maraviroc has been claimed recently to inhibit the SARS-CoV-2 S-protein mediated cell fusion in cell culture [6]. Fostemsavir, a prodrug of temsavir, which acts by blocking gp120 binding to CD4 and hence HIV attachment and entry, was approved for clinical use in the US in July 2020 as an antiretroviral for adults living with HIV/AIDS [50]. Therefore, SMIs could yield antiviral therapies that are more broadly active (i.e., less strain- and mutation-sensitive), more patient friendly (i.e., suitable for oral or inhaled administration), less immunogenic, and more controllable (shorter half-life / better biodistribution) than antibodies [51]. Oral bioavailability offers a major advantage for access, wide-spread usage, and compliance [52] – making such therapeutics more suitable for long-term and broadly acceptable preventive use [53-55] including for transmission control of viral diseases. For COVID-19, the possibility of direct delivery into the respiratory system via inhaled or intranasal administration is also important and unlikely to be achievable for antibodies. Broadly specific activity could make possible multi-strain or even pan-CoV inhibition, and while it is unlikely with antibodies [23, 24], it is possible for SMIs. For example, we have shown that while the corresponding antibodies did not cross-react for the human vs mouse CD40-CD40L PPI, our SMIs did so and had about similar potencies [56, 57].

Since previously we found that starting from organic dyes one can identify SMIs for co-signaling PPIs as potential immunomodulatory agents [51, 56-62], we initiated a screen of such compounds for their ability to inhibit the SARS-CoV-2-S–ACE2 PPI. This led to the identification of several organic dyes (**1–5**, Figure 1) that show inhibitory activity of this PPI *in vitro*, including methylene blue (**6**), a phenothiazine dye approved by the FDA for the treatment of methemoglobinemia, which we have described separately [63]. More importantly, it also led to the identification of new and more potent SMIs (**7–13**) that are more drug-like, free of color-causing chromophores, and less likely to be promiscuous protein binders as summarized below.

RESULTS

As part of our work to identify SMIs for co-signaling PPIs that are essential for the activation and control of immune cells, we discovered that the chemical space of organic

dyes, which is particularly rich in strong protein binders, offers a useful starting point. Accordingly, it seemed logical to explore it for possible inhibitors of the SARS-CoV-2 S protein – ACE2 PPI that is an essential first step for the viral entry of this novel, highly infectious coronavirus. We were able to set up a cell-free ELISA-type assay to quantify the binding of SARS-CoV-2 S protein (as well as its SARS-CoV analog) to their cognate receptor (hACE2) and used this to screen our existing in-house compound library containing a large variety of organic dyes and a set of colorless analogs prepared as potential SMIs for costimulatory PPIs. These maintain the main molecular framework of dyes but lack the aromatic azo chromophores responsible for the color as they are replaced with amide linkers [61, 62].

Chemistry and Synthesis

All new compounds used here were synthesized as described before as part of our effort to identify novel SMIs for the CD40–CD40L costimulatory PPI [61, 62]. Synthesis involved one or two amide couplings (using a modified version of the procedure from [64]) and a hydrogenation (using a modified version of the procedure from [65]). These steps were used with different linkers and naphthyl moieties as needed for each structure; all corresponding details are summarized in the Supporting Information (Supplementary Methods and Supplementary Schemes S1-S6). All structures tested here that showed promising activity (**1–13**) are summarized in Figure 1; structures of additional compounds used as controls or inactive comparators are presented in Supporting Information Supplementary Figure S1.

Screening Assays

As a first step, we explored the feasibility of setting up screening assays using a cell-free ELISA-type format similar to those used in our previous works with Fc-conjugated receptors coated on the plate and FLAG- or His-tagged ligands in the solution [56, 59-61]. Concentration-response assessments of binding to ACE2 indicated that both the S1 and RBD portions of SARS-CoV-2-S bind strongly and follow classic sigmoid patterns corresponding to the law of mass action [66] with a slightly stronger binding for RBD than S1 (Figure 2). Fitting of data gave median effective concentrations (EC_{50}s) and hence binding affinity constant (K_d) estimates of 3.7 and 14.7 nM, respectively (98 and 1125 ng/mL) – in good agreement with the specifications of the manufacturer (SinoBiological; Wayne, PA, USA) and published values indicating a low nanomolar range (4–90 nM) typically based on surface plasmon resonance (SPR) studies [5]. Because we are interested in possible broad-spectrum inhibitors, we also performed concentration-response assessments of the binding of SARS-CoV and HCoV-NL63 S proteins (using their S1&S2 and S1 domains, respectively) as they also use ACE2 as their cognate receptor. SARS-CoV bound with about similar potency as SARS-CoV-2 (13.9 nM; 1843 ng/mL), whereas HCoV-NL63 had significantly lower affinity (45.8 nM, 3610 ng/mL) (Figure 2).

Based on this, we first used this assay to screen for inhibitors of SARS-CoV-2 RBD binding, which showed the strongest affinity to hACE2. In fact, this assay setup is very similar to one recently shown to work as a specific and sensitive SARS-CoV-2 surrogate virus neutralization test based on antibody-mediated blockage of this same PPI (CoV-S–ACE2) [67]. We screened our in-house library of organic dyes plus existing analogs together with a

few additional compounds that are or have been considered of possible interest in inhibiting SAR-CoV-2 by different mechanisms of action, e.g., chloroquine, clemastine, and suramin [23, 68-71]. Screening at 5 μM indicated that most have no activity and, hence, are unlikely to interfere with the S-protein – ACE2 binding needed for viral attachment. Nevertheless, some showed activity (Supporting Information, Figure S2). Compounds showing the strongest activity, i.e., rose Bengal, erythrosine B (ErB), and phloxine B, are known promiscuous SMIs of PPIs [59]. As such, they are of no value here being nonspecific; they were included as positive controls. This screening also identified methylene blue (MeBlu, **6**), a phenothiazine dye approved by the FDA for the treatment of methemoglobinemia and also used for several other therapeutic applications in the developed world [72-74] and with additional potential for certain developing world applications such as malaria [75], as showing promising inhibitory activity for the SARS-CoV-2-S–hACE2 PPI, likely contributing to its anti-CoV activity [76, 77]; this has been discussed separately [63].

Binding Inhibition (Concentration-Response)

Next, detailed concentration-response assessments were performed to establish inhibitory activity (IC_{50}) per standard experimental guidelines in pharmacology and experimental biology [78, 79]. These confirmed that indeed several organic dyes as well as non-dye DRI compounds inhibited this PPI in a concentration-dependent manner with low micromolar IC_{50}s (Figure 3). For example, among tested dyes, Congo red (CgRd, **1**), direct violet 1 (DV1, **4**), Evans blue (EvBl, **2**), chlorazol black (ChBk, **3**), and calcomine scarlet 3B (CSc3B, **5**) had IC_{50}s of 0.99, 1.44, 2.25, 2.57, and 4.25 μM, respectively. Further, we also found several DRI compounds of low micromolar activity including some, such as DRI-C91005 (**13**) and DRI-C23041 (**8**), with even better submicromolar IC_{50}s (160 and 520 nM, respectively). For the compounds tested here, concentration dependencies were adequately described by a standard log inhibitor vs response model (i.e., a classical sigmoid binding function with a Hill slope of 1 [66]). Sunset yellow FCF (FD&C yellow #6; Supplementary Figure S1), a structurally related azo dye and an FDA approved food colorant included as a possible negative control, showed no inhibitory activity (Figure 3). Neither did, for example, naphthol blue black (NBlBk; Figure S1) another dye containing several of the structural elements of these compounds. We also included some previously described DRI compounds such as DRI-C2105041 and DRI-C2105045 (Figure S1) [62] that had very little activity here (Figure 3) to illustrate that some structural requirements are needed, and inhibition is not just due to size or nonspecific hydrophobicity.

Notably, neither chloroquine nor suramin showed inhibitory activity in this assay. We tested chloroquine, an anti-parasitic and immunosuppressive drug primarily used to prevent and treat malaria, because it was the subject of considerable controversy regarding its potential antiviral activity against SARS-CoV-2 [68]. We also tested suramin, a polysulfonated ‘colorless dye’ and an antiparasitic drug approved for the prophylactic treatment of African sleeping sickness (trypanosomiasis) and river blindness (onchocerciasis), because it was claimed to inhibit SARS-CoV-2 infection in cell culture by preventing binding or entry of the virus [71] and because it was one of the first compounds we found to inhibit the CD40–CD40L PPI [58]. On the other hand, erythrosine B (ErB, FD&C red #3), an FDA approved food colorant that we found earlier to be a promiscuous PPI inhibitor and have been using as

positive control in such assays, inhibited with an IC_{50} of 0.4 μM, similar to its activity found for other PPIs tested before (1–20 μM) [59].

For a few representative compounds, we also tested their ability to inhibit not just the binding of SARS-CoV-2-RBD but also that of SARS-CoV-2-S1 to hACE2. We obtained similar potencies; e.g., DRI-C23041 had an IC_{50} of 1.88 μM (95% CI of 1.32–2.68 μM) for S1 (Supporting Information, Figure S3) vs 0.52 μM (95% CI of 0.42–0.63 μM) for RBD (Figure 3). This confirms that these are indeed real inhibitory activities relevant for the S protein – hACE2 PPI of interest. More importantly, we also assessed the ability of selected promising compounds to inhibit the binding of SARS-CoV-S to ACE2 using a similar setup. As shown in Figure 4, several of the same compounds including organic dyes (CgRd, DV1, and others) as well as DRI compounds showed similar activity against SARS-CoV as against SARS-CoV-2. For compounds tested in this assay such as CgRd, CVN, EvBl, CSc3B, DRI-C23041, and DRI-C91005 the IC_{50}s were 3.9, 2.6, 1.3, 9.9, 3.4, and 0.24 μM (Figure 4), respectively – values that are similar to those obtained for SARS-CoV-2 inhibition (Figure 3), raising the possibility of broad-spectrum anti-CoV activity.

In such screenings, it is also important to avoid PAINS (Pan-Assay Interference compoundS) [80, 81] and to achieve not just activity but also adequate selectivity, specificity, and safety. To become promising lead candidates, small-molecule compounds are usually expected to show >30-fold selectivity over other possible pharmacological targets of interest [82, 83]. As a counter-assay, here we assessed inhibitory activity against the TNF-R1–TNF-α interaction, as we have done before [61, 62]. Most of the dyes found here to inhibit the SARS-CoV-2–ACE2 PPI (Figure 3) seem to be relatively promiscuous as they also inhibited the TNF-R1–TNF-α PPI (Figure 5A) showing only some limited selectivity (Figure 5B), e.g., 6-fold for CgRd (0.99 vs 6.0 μM) as one of the best and only 1.4-fold for DV1 (1.5 vs. 2.1 μM). On the other hand, several DRI-C compounds showed good, more than 100-fold selectivity, e.g., >400-fold for DRI-C23041 (0.52 vs 233 μM) as evidenced in the selectivity plot of Figure 5B. The symmetric DRI-C91005 seems an exception that was the most potent in all assays but showed no selectivity (0.16 vs 0.16 μM). As these DRI-C compounds were designed to target CD40–CD40L, they all inhibit that PPI with high nanomolar – low micromolar potency and have been found to show selectivity versus other TNF superfamily PPIs [61, 62] (see Discussion).

Binding Partner (Protein Thermal Shift)

As an additional binding assay and to establish whether these SMIs bind to CoV-S or ACE2, we used a protein thermal shift (differential scanning fluorimetry or ThermoFluor) assay [84, 85] as we did before for CD40L [62]. This assay quantifies the shift in protein stability caused by binding of a ligand via use of a dye whose fluorescence increases when exposed to hydrophobic surfaces, which happens as the protein starts to unfold as it is heated and exposes its normally buried hydrophobic core residues. It allows rapid and inexpensive evaluations of the temperature-dependence of protein stability using real-time PCR instruments and only small amounts of protein. It is sensitive enough to assess small-molecule PPI interference and can be used even as a screening assay [86]. As shown in Figure 6, the presence of CgRd or DRI-C23041 caused clear left-shifts in the melting temperature

(T_m) of the protein for SARS-CoV-2-RBD, but not ACE2 (purple vs. blue lines) indicating the former as the binding partner. This is encouraging, as SMIs targeting the S-protein are much more likely to (1) not cause undesirable side effects than ACE2-targeting ones, which could interfere with ACE2 signaling, and (2) be more broadly specific due to the structural similarity of the different CoV S glycoproteins. Binding of a ligand usually results in an increase (right-shift) of the melting temperature due to stabilization of the protein; however, cases with a decrease (hence, destabilization) have also been reported [87] including for the Ebola virus glycoprotein [88].

Inhibition of SARS-CoV-2 Pseudo-Virus Entry

For a set of selected active compounds, we were able to confirm that they also inhibit viral entry using two different pseudovirus assays. First, it has been done with a baculovirus pseudotyped with spike proteins, i.e., bearing the SARS-CoV-2 S (plus fluorescent reporters) and generated using BacMam-based tools. These allow quantification of viral entry, as they express bright green fluorescent protein that is targeted to the nucleus of ACE2- (and red fluorescence reporter) expressing host cells (here, HEK293T), but can be handled using biosafety level 1 containment, as they do not replicate in human cells. A day after entry, host cells express green fluorescence in the nucleus, indicating pseudovirus entry. If entry is blocked, the cell nucleus remains dark. In this assay, several of our SMIs tested, for example, CgRd, DV1, and DRI-C23041 showed good concentration-dependent inhibition as illustrated by the corresponding images and bar graphs in Figure 7. Fitting with regular concentration response curves indicated a very encouraging IC_{50} of 5.8 μM for DRI-C23041. CgRd and DV1 also inhibited, but with higher IC_{50}s (26 and 64 μM for, respectively), which is not unexpected for such azo dyes as they tend to lose activity in cell-based assay due to nonspecific binding (Figure 7C). In the meantime, hydroxychloroquine (Figure 7C), NBlBk, and DRI-C2105041 (data not shown) did not show any significant inhibition even at the highest concentration tested (45 μM).

A second confirmatory assay has been done with a different pseudovirus (SARS-CoV-2 spike plus GFP reporter bearing VSV-ΔG pseudovirus, i.e., vesicular stomatitis virus that lacks the VSV envelope glycoprotein) [89] and cell line (ACE2/Furin-overexpressing Vero-E6 cells). GFP fluorescence quantified using a live imaging system (Incucyte) was used as a measure of infection, and normalized values were fitted with regular concentration response curves as before. Obtained inhibitory effects (Figure 8) were very consistent with those from the previous assay with IC_{50}s of 7.4, 27, and 16 μM for DRI-C23041, CgRd, and DV1, respectively confirming the antiviral potential of these compounds.

As a first safety assessment, in parallel with the cell assays, we also evaluated cytotoxicity for several compounds in the same cells and at the same concentrations using a standard MTS assay to ensure that effects are present at non-toxic concentration levels. Notably, chloroquine already showed noticeable cytotoxicity at 45 μM concentrations in this assay with HEK293T cells, so its effect on pseudovirus entry could not be reliably evaluated there and hydroxychloroquine was used. We have shown before that compounds such as DRI-C21041 (**7**) or DRI-C24041 (**9**) did not have significant effects on the viability of THP-1 human cells for concentrations of up to 200 μM [61, 62]. In line with that, DRI-C23041

(**8**) was the least cytotoxic among tested compounds here and showed no significant effects on HEK293T at 45 μM (Supporting Information, Figure S4), whereas it had a strong effect on viral entry (Figure 7).

DISCUSSION

Results obtained here confirm again that the chemical space of organic dyes can serve as a useful starting platform for the identification of SMI scaffolds for PPI inhibition. Organic dyes need to be good protein binders; hence, their contain privileged structures for protein binding [90-92] and can provide a better starting point toward the identification of SMIs of PPIs than most drug-like screening libraries, whose chemical space has been shown to not correspond well with that of promising PPI inhibitors [93-95]. Using this strategy, we have identified promising SMIs for the CD40–CD40L costimulatory interaction [56, 61, 62] and even some promiscuous SMIs of PPIs [59]. Of course, because most dyes are unsuitable for therapeutic applications due to their strong color and, in the case of azo dyes, their quick metabolic degradation [96, 97], structural modifications are needed to optimize their clinical potential [61, 62].

Here, we explored the potential of this approach to identify SMIs for the PPI between ACE2 and CoV spike proteins as potential antivirals inhibiting attachment. Since SARS-CoV-2 uses its S protein via its RBD to bind ACE2 as the first step of its entry [3, 5, 13, 14], targeting these proteins is a viable therapeutic strategy, and work with prior zoonotic CoV has demonstrated proof-of-concept validity for such approaches. By screening our compound library spanning the chemical space of organic dyes, we identified several promising SMIs including dyes, such as Congo red and direct violet 1, as well as novel drug-like compounds, such as DRI-C23041, that *(1)* inhibited the SARS-CoV-2-S–hACE2 PPI with low micromolar activity (Figure 3), *(2)* seem to bind to SARS-CoV-2-S and not ACE2 (Figure 6), and *(3)* inhibited entry of two different SARS-CoV-2-S displaying pseudoviruses into ACE2 expressing HEK293T and ACE2/Furin over-expressing Vero-E6 cells (Figure 7, Figure 8). Importantly, there is clear indication of a consensus structural motif present in the active compounds identified here: a biphenyl linker with a naphthyl at one end and another aromatic naphthyl or phenyl at the other end, both with at least one but preferably multiple polar substituents (Figure 1).

Since many azo-containing dyes are likely PAINS (pan-assay interference compounds) and could be false positives in screening assays [80, 81], we have checked in a number of previous works that the PPI inhibitory activity seen is not due to polymolecular conglomeration [98, 99] / aggregation [100, 101], a frequent cause of promiscuous inhibition, by adding a non-ionic detergent (Triton-X 100, 0.01%) to the binding inhibitory assay as recommended for the detection of such effects [102]. This was found to have no significant effect for several dyes inhibiting the CD40–CD40L PPI [56], not even ErB [59], as well as for all DRI-C compounds tested [61, 62]. The presence of Triton also caused no significant deterioration in the inhibitory effects on SARS-CoV-2 RBD binding here; for example, IC_{50}s changed from 0.52 μM (95% CI: 0.42–0.63) to 0.85 μM (95% CI: 0.62–1.18) for DRI-C23041 and from 0.99 μM (95% CI: 0.63–1.59) to 1.99 μM (95% CI: 1.16–3.43) for CgRd. It is increasingly recognized that PAINS filters / alerts have to be used cautiously and only in combination with orthogonal

assays for selectivity, as many PAINS may still provide useful activity/information, 97% of them were found to be infrequent hitters in PPI inhibitory assays, and about ~7% of the approved drugs are actually PAINS [103-105]. Dyes identified here indeed do not show much selectivity and are likely promiscuous protein binders. However, DRI-C compounds, especially DRI-C23041 do not raise any PAINS-alert when tested in recommended *in silico* filters, have activity confirmed in two independent protein-based assays (ELISA and thermal shift) plus a pseudo-virus assay – all with well-behaved concentration–response curves (i.e., unity Hill coefficients $n_{Hill} = 1$), and show >100-fold selectivity in inhibition versus that in the TNF counter-screen (Figure 5B).

Following the emergence of SARS-CoV in the early 2000s, a limited number of groups performed high-throughput screening (HTS) assays to identify inhibitory drug candidates for targeting various early steps in its cell invasion. Identified candidates included some putative SMIs of viral entry, for example, SSAA09E2 [106] and VE607 [107]. Inhibitory candidates acting by other mechanism identified included, for example, SSAA09E1, SSAA09E3 [106]; MP576, HE602 [107]; ARB 05-018137, ARB 05-090614 [108]; KE22 [109]; and others (reviewed in [23, 33, 34]). Most of these showed activities only in the low micromolar range, e.g., 3.1, 0.7, and 1.6 μM for SSAA09E2, K22, and VE607, respectively [23]. Even if these compounds showed some evidence of inhibiting CoV infection, no approved preventive or curative therapy is currently available for human CoV diseases. In addition to the relatively low (micromolar) potency, a main reason for this is that these compounds were not suitable for clinical translatability. They could not pass the pre-clinical development stage and enter clinical trials due to their poor bioavailability, safety, and pharmacokinetics [23]. Note that by starting from a different chemical space and not from that of drug-like molecules typically used for HTS, our best SMIs identified here are already well within this low micromolar range for SARS-CoV-2. There also was a recent attempt at identifying possible disruptors of the SARS-CoV-2-S-RBD–ACE2 binding using AlphaLISA assay based HTS of 3,384 small-molecule drugs and pre-clinical compounds suitable for repurposing that identified 25 possible hits [110]. However, these were also of relatively low potency (micromolar IC_{50}s). None of them shows resemblance with the scaffold(s) identified here – highlighting again the known lack of overlap between the chemical space of existing drugs / drug-like structures and that of PPI inhibitors.

The S protein is a homotrimer with each of its monomer units being about 180 kDa, and it contains two subunits, S1 and S2, mediating cell attachment and fusion of the viral and cellular membrane, respectively [17, 111]. The RBD of the S protein is located within the S1 domain and is known to switch between a standing-up position for receptor binding and a lying-down position for immune evasion [13, 33]. CoVs can utilize different receptors for binding, but several CoVs, even from different genera, can also utilize the same receptor. SARS-CoV-2 is actually the third human CoV utilizing ACE2 as its cell entry receptor, the other two being SARS-CoV and the α-coronavirus HCoV NL63 [3]. MERS-CoV recognizes dipeptidyl peptidase 4 (DPP4) [3-5], while HCoV 229E recognizes CD13 [112]. Some β-coronaviruses (e.g., HCoV OC43) bind to sialic acid receptors [113]. Having access to broadly cross-reactive agents that can neutralize a wide range of antigenically disparate viruses that share similar pathogenic outcomes would be highly valuable from a therapeutic perspective [18], and SMIs are less specific and could yield therapies that are more broadly

active (i.e., less strain- and mutation-sensitive) than antibodies, which tend to be highly specific. We have shown before that while the corresponding antibodies are species specific for the CD40–CD40L PPI, our SMIs could inhibit both the human and mouse system with similar potencies [56, 57]. Hence, it is feasible that SMI structures can be identified that in addition to inhibiting SARS-CoV-2, also inhibit other CoVs, including the high lethality SARS-CoV and MERS-CoV as well as the common cold causing HCoVs. Along these lines, it is very encouraging that SMIs identified here target the CoV-S protein and not ACE2 (Figure 6) and they show similar potency in inhibiting SARS-CoV (Figure 4) and SARS-CoV-2 (Figure 3). Such inhibitory effects on viral attachment can translate into antiviral activity against SARS-CoV-2 and possibly other ACE2-binding CoVs such as SARS-CoV and the α-coronavirus HCoV NL63.

While the SMIs identified here are not very small structures (MW in the 550 to 700 Da range), they are still relatively small compared to typical SMIs of PPIs. These tend to have larger structures to achieve sufficient activity, and they often severely violate the widely used “rule-of-five” criteria, which, among others, requires MW < 500 [114]. In the last two decades, this “rule” has been used as a guide to ensure oral bioavailability and an adequate pharmacokinetic profile. Nevertheless, an increasing number of new drugs have been launched recently (including the two small-molecule PPI inhibitors discussed earlier) that significantly violate these empirical rules proving that oral bioavailability can be achieved even in the “beyond rule-of-five” chemical space [115]. Hence, our results provide further proof for the feasibility of SMI for CoV attachment and provide a first map of the chemical space needed to achieve this.

Finally, these DRI-C structures (**8–13**) were originally intended to modulate co-signaling interactions, specifically to inhibit the CD40–CD40L costimulatory interaction, and they do so with low micromolar potency in cell assays (≈10 μM) [61, 62]. While some show good selectivity vs TNF (e.g., DRI-C23041, DRI-C24041), others seem more promiscuous (e.g., DRI-C91005). TNF-inhibitory activities here were somewhat stronger than those we obtained before, e.g., IC_{50}s of 0.6 vs 5 [59] for ErB or 181 vs >1000 [62] for DRI-C21041, possibly due to the use of a different blocking buffer. We hope that these PPI inhibitory activities can be ultimately separated, but even if not and they still retain some activity in modulating co-signaling interactions, this might not necessarily be counterproductive. It could provide a unique opportunity to pursue dual-function molecules that on one hand, have antiviral activity by inhibiting the interaction needed for CoV attachment (e.g., SARS-CoV-2-S–ACE2) and, on the other, possess immunomodulatory activity to rein-in overt inflammation (inhibiting CD40–CD40L) or to unleash T cell cytotoxicity against virus-infected cells (inhibiting PD-1–PD-L1). Targeting of the PD-1 co-signaling pathway could be particularly valuable for its potential in restoring T cell homeostasis and function from an exhausted state [116, 117], which is of interest to improve viral clearance and rein-in the inflammatory immune response and the associated cytokine storm during anti-viral responses such as those likely implicated in the serious side effects seen in many COVID-19 patients [1, 118-120]. Notably, the overexuberant immune response seen in COVID-19 has raised the possibility that the lethality related to infection with the SARS-CoV-2 is possibly related to an uncontrolled autoimmune response induced by the virus [121], and the presence

of auto-antibodies against type I IFNs in patients with life-threatening COVID-19 has now been confirmed [122].

In conclusion, screening of our library of organic dyes and related novel drug-like compounds led to the identification of several small-molecule compounds showing promising broad-spectrum inhibition of the PPI between coronavirus spike proteins and their cognate ACE2 receptor. For several of them, including dyes, such as Congo red and direct violet 1, but especially novel non-dye compounds, such as DRI-C23041, we have confirmed that they are able to inhibit the entry of SARS-CoV-2-S expressing pseudoviruses into ACE2-expressing cells in a concentration-dependent manner. While specificities and activities might require further optimization, these results provide clear proof-of-principle evidence that this PPI, critical for CoV attachment and entry, is susceptible to small-molecule inhibition, making it feasible to pursue such alternative therapeutic options for the prevention and treatment of COVID-19 as oral or inhaled medications.

METHODS

Commercial grade reagents and solvents were purchased from VWR (Radnor, PA, USA) and Sigma-Aldrich (St. Louis, MO, USA) and directly used without further purification. Chemicals, reagents, and the overwhelming majority of compounds used here were obtained from Sigma-Aldrich (St. Louis, MO, USA) and used as such; purity values are available on the manufacturer website. Some organic dyes (e.g., acid brown M, direct violet 1, and chlorazol black BH) were from TCI America (Portland, OR, USA); direct red 80 was from Santa Cruz Biotechnology (Dallas, TX, USA); gallein, NF023, and suramin were from Tocris Bioscience (Biotechne, Minneapolis, MN, USA). For compounds purchased and assessed as such in detail (concentration-response), purities (and catalog numbers) were as follows: erythrosine B 90% (198269), sunset yellow FCF 90% (465224), naphthol blue black >99% (70490), Congo red 85% (860956), Evans blue 85% (206334), chlorazol black >99% (C1144), calcomine scarlet 3B >90% (S479284), methylene blue >95% (M4159), chloroquine >98.5% (C6628), and hydroxychloroquine >98% (H0915) – all from Sigma Aldrich; direct violet 1 >99% (C0551) from TCI America; and suramin >99% (1472) from Tocris Bioscience (Biotechne).

Chemistry

General methods—All reactions were carried out in oven- or flame-dried glassware under an atmosphere of dry argon (unless otherwise noted) and were magnetically stirred and monitored by analytical thin-layer chromatography (TLC) using Merck (Kenilworth, NJ, USA) pre-coated silica gel plates with F_{254} indicator (except if otherwise indicated). Visualization was accomplished by UV light (256 nm) with a combination of potassium permanganate and/or vanillin solution as an indicator. Flash column chromatography was performed according to the method of Still [123] using silica gel 60 (mesh 230-400; EMD Millipore, Billerica, MA, USA).

All newly synthesized compounds were characterized with ^{1}H NMR, ^{13}C NMR, high-resolution mass spectrometry (HRMS), and infrared (IR) spectroscopy – detailed data are provided in the Supporting Information. Chemical shifts are reported in ppm relative

to TMS. DMSO-d_6 (2.50 ppm) was used as a solvent for ^{1}H NMR and ^{13}C NMR. ^{1}H NMR and ^{13}C NMR spectra were recorded on Bruker Avance 300 (300 MHz ^{1}H), 400 (400 MHz ^{1}H, 100 MHz ^{13}C), and 500 (500 MHz ^{1}H, 125 MHz ^{13}C). Chemical shift values (δ) are reported in ppm relative to Me_4Si (δ 0.0 ppm) unless otherwise noted. Proton spectra are reported as δ (multiplicity, coupling constant *J*, number of protons). Multiplicities are indicated by *s* (singlet), *d* (doublet), *t* (triplet), *q* (quartet), *p* (quintet), *h* (septet), *m* (multiplet), and *br* (broad). IR spectra were recorded with a FT-IR spectrophotometer Paragon 1000 (PerkinElmer). Mass spectra were obtained at the Mass Spectrometry Research and Education Center, Department of Chemistry, University of Florida (Gainesville, FL, USA). Low-resolution ES (electron spray) mass spectra were carried out with Finnigan LCQ DECA/Agilent 1100 LC/MS mass spectrometer (Thermo Fisher Scientific, Waltham, MA, USA). High-resolution mass spectra were recorded on an Agilent 6220 ESI TOF (Santa Clara, CA, USA) mass spectrometer. Analysis of sample purity was performed on an Agilent (Palo Alto, CA, USA) 1100 series HPLC system with a Thermoscientific Hypurity C8 (5 μm; 2.1 × 100 mm + guard column). HPLC conditions were as follows: solvent A = water with 2 mM ammonium acetate, solvent B = methanol with 2 mM ammonium acetate, and flow rate = 0.2 mL/min. Compounds were eluted with a gradient of A/B = 80:20 at 0 min to 0:100 at 50 min. Purity was determined via integration of UV spectra at 254 nm, and all tested compounds have a purity of >95%. All synthesized target compounds were tested as triethylamine salts unless otherwise stated. Details of the synthesis and structure conformation for all DRI-C compounds used here are summarized in the Supporting Information (Supplementary Methods and Supplementary Schemes S1-S6).

Binding Assays

SARS-CoV-2 S1 and RBD (cat. no. 40591-V08H and 40592-V08H), SARS-CoV S1+S2 (cat. no. 40634-V08B), HCoV-NL63 S1 (cat. no. 40600-V08H; all with His tag) and ACE2-Fc (cat. no. 10108-H05H) used in the binding assay were obtained from SinoBiological (Wayne, PA, USA). The TNF-R1:Fc receptor (cat. no. ALX-522-013-C050) and its FLAG-tagged TNF-α ligand (cat. no. ALX-522-008-C050) were obtained from Enzo Life Sciences (San Diego, CA, USA). Binding inhibition assays were performed in a 96-well cell-free format similar to the one described before [56, 59-61]. Briefly, microtiter plates (Nunc F Maxisorp, 96-well; Thermo Fisher Scientific, Waltham, MA, USA) were coated overnight at 4 °C with 100 μL/well of Fc-conjugated ACE2 receptor diluted in PBS pH 7.2. This was followed by blocking with 200 μL/well of SuperBlock (PBS) (Thermo Fisher Scientific) for 1 h at RT [63]. Then, plates were washed twice using washing solution (PBS pH 7.4, 0.05% Tween-20) and tapped dry before the addition of the tagged ligand (SARS-CoV-2 S1 or RBD) and test compounds diluted in binding buffer (20 mM HEPES, pH 6.8) to give a total volume of 100 μL/well. After 1 h incubation, three washes were conducted, and a further 1 h incubation with anti-His HRP conjugate (BioLegend; San Diego, CA, USA; cat. no. 652504) diluted (1:2500) in SuperBlock (PBS) was used to detect the bound His-tagged ligand. Plates were washed four times before the addition of 100 μL/well of HRP substrate TMB (3,3′,5,5′-tetramethylbenzidine) and kept in the dark for up to 15 min. The reaction was stopped using 20 μL of 1M H_2SO_4, and the absorbance value was read at 450 nm. The plated concentrations of ACE2 receptor and corresponding concentrations of the ligand used in the inhibitory assays were: 1.0 μg/mL ACE2 with 0.5 μg/mL SARS-CoV-2 RBD, 2.0

μg/mL ACE2 with 1.5 μg/mL SARS-CoV-2 S1, and 1.0 μg/mL ACE2 with 1 μg/mL SARS-CoV S1S2. These values were selected following preliminary testing to optimize response (i.e., to produce a high-enough signal at conditions close to half-maximal response, EC_{50}). As before [56, 59, 61, 62], to verify that inhibition is not due to colloidal aggregation, RBD binding inhibition was also measured in the presence of the non-ionic detergent Triton-X 100 (0.01%), as recommended for the detection of such effects [80, 102]. Binding assessments for TNF-R1–TNF-α were performed as previously described using TNF-R1 at 0.3 μg/mL and TNF-α at 0.02 μg/mL [62], with the exception of using SuperBlock as the blocking buffer here. Stock solutions of compounds at 10 mM in DMSO were used.

Protein Thermal Shift (Differential Scanning Fluorimetry)

This assay was used as described before [62] and following standard protocols from literature [84, 85] to establish which protein binds our compounds. SYPRO Orange (ThermoFisher; Waltham, MA, USA) was used as the fluorescence detection dye with an RT-PCR machine (StepOnePlus, Applied Biosystems, Foster City, CA, USA; detection on ROX channel, 575/602 nm) programmed to equilibrate samples at 25 °C for 90 s and then increase temperature to 99 °C by 0.4 °C every 24 s before taking a reading. Melting point of the protein is considered the lowest point of the first derivative plot, as calculated by the software included with the RT-PCR machine. Optimal concentrations were determined by performing a series of preliminary scans at various concentrations of protein, compound, and dye (SARS-CoV-2-RBD 0.05 mg/mL, hACE2-Fc 0.05 mg/mL, SYPRO Orange 4×, 100 mM HEPES buffer, 10 μM of test compound).

SARS-CoV-2 Pseudovirus Assays

For the BacMam based assay, fluorescent biosensors from Montana Molecular (Bozeman, MT, USA; cat. no. C1100R and C1100G) were used per the instructions of the manufacturer with minor modifications. Briefly, HEK293T cells (ATCC, Manassas, VA, USA; cat. no. CRL-3216) were seeded onto 96-well plates at a density of 50,000 cells per well in 100 μL complete medium (DMEM supplemented with 10% fetal bovine serum). A transduction mixture containing ACE2 BacMam Red-Reporter virus (1.8×10^8 Vg/mL) and 2 mM sodium butyrate prepared in complete medium was added (50 μL per well) and incubated for 24 h at 37°C and 5% CO_2. Medium was removed, washed once with PBS, and replaced with 100 μL fresh medium containing the compound under study, pre-incubating for 30 min at 37°C and 5% CO_2. A transduction mixture containing Pseudo SARS-CoV-2 Green-Reporter pseudovirus (3.3×10^8 Vg/mL) and 2 mM sodium butyrate prepared in complete medium was added (50 μL per well) and incubated for 48 h at 37°C and 5% CO_2. Medium was removed, washed once with PBS, replaced with 150 μL fresh medium, and cells incubated for additional 48 h at 37°C and 5% CO_2. Cell fluorescence was detected using an EVOS FL microscope (Life Technologies, Carlsbad, CA, USA) and quantified using the Analyze Particles tool after thresholding for the corresponding colors in ImageJ (US National Institutes of Health, Bethesda, MD, USA; [124]).

For the VSV-ΔG based assay, the SARS-CoV-2 S bearing pseudovirus generated in-house was used as described before [89]. Vero-E6 cells (African Green Monkey renal epithelial cells; ATCC cat. no. CRL-1586) engineered to overexpress hACE2/Furin were seeded in 24-well

plates to obtain a confluence of 80%. The medium was replaced with 250 μL cell culture medium (DMEM) supplemented with 2% Fetal Bovine Serum, 1% Penicillin/Streptomycin/Glutamine, and the compounds of interest for 30 min. Cells were inoculated with the SARS-CoV-2 spike protein pseudotyped VSV-ΔG (multiplicity of infection = 0.05) by adding complete media to bring the final volume to 400 μL, and 20 h post infection, plates were scanned with a 10× objective using the Incucyte ZOOM imaging system (Sartorius, Ann Arbor, MI, USA). Normalized GFP expression (GCU) values per image were obtained by dividing the Total Green Object Integrated Intensity [Green Calibrated Units (GCU) × μm^2/image] values of each image by its corresponding Total Phase Area (μm^2/image) as described before [89].

Cytotoxicity Assay

For the MTS assay, HEK293T cells were cultured and prepared in the same manner as for the pseudovirus assay (up until the removal of test compounds there). Briefly, cells were added to a 96-well microtiter plate at a density of 50,000 cells/well in the absence or presence of various concentrations of compounds diluted in the same media. The plate was incubated at 37°C for 48 h. After washing three times with culture media, 20 μL per well of MTS, 3-(4,5-dimethylthiazol-2-yl)-5-(3-carboxymethoxyphenyl)-2-(4-sulfophenyl)-2H-tetrazolium, (Promega, Madison, WI, USA) was added to the plate at a final volume of 200 μL, and cells were incubated at 37°C for 2 h. Formazan levels were measured using a plate reader at 490 nm.

Statistics and Data Fitting

All binding inhibition assays were performed as at least duplicates per plates, and all results shown are average of at least two independent experiments. As before [59-61], binding data were converted to percent inhibition and fitted with standard log inhibitor vs. normalized response models [66] using nonlinear regression in GraphPad Prism (GraphPad, La Jolla, CA, USA) to establish half-maximal effective or inhibitory concentrations (EC_{50}, IC_{50}).

Supplementary Material

Refer to Web version on PubMed Central for supplementary material.

ACKNOWLEDGMENTS

Financial support by the Diabetes Research Institute Foundation (www.diabetesresearch.org) is gratefully acknowledged. We thank the Mass Spectrometry Research and Education Center at the University of Florida (supported by funding from NIH S10 OD021758-01A1) for their prompt and professional service.

ABBREVIATIONS:

ACE2	angiotensin converting enzyme 2
CoV	coronavirus
PPI	protein-protein interaction
SARS	severe acute respiratory syndrome

SMI small-molecule inhibitor.

REFERENCES

(1). Liu PP; Blet A; Smyth D; Li H The science underlying COVID-19: implications for the cardiovascular system. Circulation 2020, 142, 68–78. [PubMed: 32293910]

(2). Moore JB; June CH Cytokine release syndrome in severe COVID-19. Science 2020, 368 (6490), 473–474. [PubMed: 32303591]

(3). Matheson NJ; Lehner PJ How does SARS-CoV-2 cause COVID-19? Science 2020, 369 (6503), 510–511. [PubMed: 32732413]

(4). Tiwari V; Beer JC; Sankaranarayanan NV; Swanson-Mungerson M; Desai UR Discovering small-molecule therapeutics against SARS-CoV-2. Drug Discov. Today 2020, 25 (8), 1535–1544. [PubMed: 32574699]

(5). Sivaraman H; Er SY; Choong YK; Gavor E; Sivaraman J Structural basis of the SARS-CoV-2/SARS-CoV receptor binding and small-molecule blockers as potential therapeutics. Annu. Rev. Pharmacol. Toxicol 2020, ePub.

(6). Risner KH; Tieu KV; Wang Y; Bakovic A; Alem F; Bhalla N; Nathan S; Conway DE; Macklin P; Narayanan A Maraviroc inhibits SARS-CoV-2 multiplication and s-protein mediated cell fusion in cell culture. bioRxiv 2020, 2020.08.12.246389.

(7). Guy RK; DiPaola RS; Romanelli F; Dutch RE Rapid repurposing of drugs for COVID-19. Science 2020, 368 (6493), 829–830. [PubMed: 32385101]

(8). Rajgor DD; Lee MH; Archuleta S; Bagdasarian N; Quek SC The many estimates of the COVID-19 case fatality rate. Lancet Infect. Dis 2020, 20 (7), 776–777. [PubMed: 32224313]

(9). Salje H; Tran Kiem C; Lefrancq N; Courtejoie N; Bosetti P; Paireau J; Andronico A; Hoze N; Richet J; Dubost CL; Le Strat Y; Lessler J; Levy-Bruhl D; Fontanet A; Opatowski L; Boelle PY; Cauchemez S Estimating the burden of SARS-CoV-2 in France. Science 2020, 369 (6500), 208–211. [PubMed: 32404476]

(10). O'Driscoll M; Ribeiro Dos Santos G; Wang L; Cummings DAT; Azman AS; Paireau J; Fontanet A; Cauchemez S; Salje H Age-specific mortality and immunity patterns of SARS-CoV-2. Nature 2021, 590 (7844), 140–145. [PubMed: 33137809]

(11). WHO Solidarity Trial Consortium; Pan H; Peto R; Henao-Restrepo AM; Preziosi MP; Sathiyamoorthy V; Abdool Karim Q; Alejandria MM; Hernandez Garcia C; Kieny MP; Malekzadeh R; Murthy S; Reddy KS; Roses Periago M; Abi Hanna P; Ader F; Al-Bader AM; Alhasawi A; Allum E; Alotaibi A; Alvarez-Moreno CA; Appadoo S; Asiri A; Aukrust P; Barratt-Due A; Bellani S; Branca M; Cappel-Porter HBC; Cerrato N; Chow TS; Como N; Eustace J; Garcia PJ; Godbole S; Gotuzzo E; Griskevicius L; Hamra R; Hassan M; Hassany M; Hutton D; Irmansyah I; Jancoriene L; Kirwan J; Kumar S; Lennon P; Lopardo G; Lydon P; Magrini N; Maguire T; Manevska S; Manuel O; McGinty S; Medina MT; Mesa Rubio ML; Miranda-Montoya MC; Nel J; Nunes EP; Perola M; Portoles A; Rasmin MR; Raza A; Rees H; Reges PPS; Rogers CA; Salami K; Salvadori MI; Sinani N; Sterne JAC; Stevanovikj M; Tacconelli E; Tikkinen KAO; Trelle S; Zaid H; Rottingen JA; Swaminathan S Repurposed antiviral drugs for Covid-19 - Interim WHO Solidarity trial results. N. Engl. J. Med 2020, ePub.

(12). Melby T; Westby M Inhibitors of viral entry. Handb. Exp. Pharmacol 2009, 189, 177–202.

(13). Shang J; Wan Y; Luo C; Ye G; Geng Q; Auerbach A; Li F Cell entry mechanisms of SARS-CoV-2. Proc. Natl. Acad. Sci. U.S.A 2020, 117 (21), 11727–11734. [PubMed: 32376634]

(14). Lan J; Ge J; Yu J; Shan S; Zhou H; Fan S; Zhang Q; Shi X; Wang Q; Zhang L; Wang X Structure of the SARS-CoV-2 spike receptor-binding domain bound to the ACE2 receptor. Nature 2020, 581 (7807), 215–220. [PubMed: 32225176]

(15). Tai W; He L; Zhang X; Pu J; Voronin D; Jiang S; Zhou Y; Du L Characterization of the receptor-binding domain (RBD) of 2019 novel coronavirus: implication for development of RBD protein as a viral attachment inhibitor and vaccine. Cell. Mol. Immunol 2020, 17 (6), 613–620. [PubMed: 32203189]

(16). Lv Z; Deng YQ; Ye Q; Cao L; Sun CY; Fan C; Huang W; Sun S; Sun Y; Zhu L; Chen Q; Wang N; Nie J; Cui Z; Zhu D; Shaw N; Li XF; Li Q; Xie L; Wang Y; Rao Z; Qin CF; Wang

X Structural basis for neutralization of SARS-CoV-2 and SARS-CoV by a potent therapeutic antibody. Science 2020, 369 (6510), 1505–1509. [PubMed: 32703908]

(17). Wang C; Li W; Drabek D; Okba NMA; van Haperen R; Osterhaus A; van Kuppeveld FJM; Haagmans BL; Grosveld F; Bosch BJ A human monoclonal antibody blocking SARS-CoV-2 infection. Nat. Commun 2020, 11 (1), 2251. [PubMed: 32366817]

(18). Sui J; Deming M; Rockx B; Liddington RC; Zhu QK; Baric RS; Marasco WA Effects of human anti-spike protein receptor binding domain antibodies on severe acute respiratory syndrome coronavirus neutralization escape and fitness. J. Virol 2014, 88 (23), 13769–13780. [PubMed: 25231316]

(19). Wu Y; Wang F; Shen C; Peng W; Li D; Zhao C; Li Z; Li S; Bi Y; Yang Y; Gong Y; Xiao H; Fan Z; Tan S; Wu G; Tan W; Lu X; Fan C; Wang Q; Liu Y; Zhang C; Qi J; Gao GF; Gao F; Liu L A noncompeting pair of human neutralizing antibodies block COVID-19 virus binding to its receptor ACE2. Science 2020, 368 (6496), 1274–1278. [PubMed: 32404477]

(20). Yuan M; Liu H; Wu NC; Lee CD; Zhu X; Zhao F; Huang D; Yu W; Hua Y; Tien H; Rogers TF; Landais E; Sok D; Jardine JG; Burton DR; Wilson IA Structural basis of a shared antibody response to SARS-CoV-2. Science 2020, 369 (6507), 1119–1123. [PubMed: 32661058]

(21). Wec AZ; Wrapp D; Herbert AS; Maurer DP; Haslwanter D; Sakharkar M; Jangra RK; Dieterle ME; Lilov A; Huang D; Tse LV; Johnson NV; Hsieh CL; Wang N; Nett JH; Champney E; Burnina I; Brown M; Lin S; Sinclair M; Johnson C; Pudi S; Bortz R 3rd; Wirchnianski AS; Laudermilch E; Florez C; Fels JM; O'Brien CM; Graham BS; Nemazee D; Burton DR; Baric RS; Voss JE; Chandran K; Dye JM; McLellan JS; Walker LM Broad neutralization of SARS-related viruses by human monoclonal antibodies. Science 2020, 369 (6504), 731–736. [PubMed: 32540900]

(22). Liu Z; Xiao X; Wei X; Li J; Yang J; Tan H; Zhu J; Zhang Q; Wu J; Liu L Composition and divergence of coronavirus spike proteins and host ACE2 receptors predict potential intermediate hosts of SARS-CoV-2. J. Med. Virol 2020, 92 (6), 595–601. [PubMed: 32100877]

(23). Xiu S; Dick A; Ju H; Mirzaie S; Abdi F; Cocklin S; Zhan P; Liu X Inhibitors of SARS-CoV-2 entry: current and future opportunities. J. Med. Chem 2020, 63 (21), 12256–12274. [PubMed: 32539378]

(24). Ju B; Zhang Q; Ge J; Wang R; Sun J; Ge X; Yu J; Shan S; Zhou B; Song S; Tang X; Yu J; Lan J; Yuan J; Wang H; Zhao J; Zhang S; Wang Y; Shi X; Liu L; Zhao J; Wang X; Zhang Z; Zhang L Human neutralizing antibodies elicited by SARS-CoV-2 infection. Nature 2020, 584, 115–119. [PubMed: 32454513]

(25). Kondo T; Iwatani Y; Matsuoka K; Fujino T; Umemoto S; Yokomaku Y; Ishizaki K; Kito S; Sezaki T; Hayashi G; Murakami H Antibody-like proteins that capture and neutralize SARS-CoV-2. Sci. Adv 2020, 6 (42), eabd3916. [PubMed: 32948512]

(26). Baum A; Fulton BO; Wloga E; Copin R; Pascal KE; Russo V; Giordano S; Lanza K; Negron N; Ni M; Wei Y; Atwal GS; Murphy AJ; Stahl N; Yancopoulos GD; Kyratsous CA Antibody cocktail to SARS-CoV-2 spike protein prevents rapid mutational escape seen with individual antibodies. Science 2020, 369 (6506), 1014–1018. [PubMed: 32540904]

(27). Wibmer CK; Ayres F; Hermanus T; Madzivhandila M; Kgagudi P; Lambson BE; Vermeulen M; van den Berg K; Rossouw T; Boswell M; Ueckermann V; Meiring S; von Gottberg A; Cohen C; Morris L; Bhiman JN; Moore PL SARS-CoV-2 501Y.V2 escapes neutralization by South African COVID-19 donor plasma. Nat. Med 2021, 27, 622–625. [PubMed: 33654292]

(28). Leader B; Baca QJ; Golan DE Protein therapeutics: a summary and pharmacological classification. Nat. Rev. Drug Discov 2008, 7 (1), 21–39. [PubMed: 18097458]

(29). Suntharalingam G; Perry MR; Ward S; Brett SJ; Castello-Cortes A; Brunner MD; Panoskaltsis N Cytokine storm in a phase 1 trial of the anti-CD28 monoclonal antibody TGN1412. N. Engl. J. Med 2006, 355 (10), 1018–1028. [PubMed: 16908486]

(30). Wadman M London's disastrous drug trial has serious side effects for research. Nature 2006, 440 (7083), 388–389. [PubMed: 16554763]

(31). Huck BR; Kötzner L; Urbahns K Small molecules drive big improvements in immuno-oncology therapies. Angew. Chem. Int. Ed. Engl 2018, 57 (16), 4412–4428. [PubMed: 28971564]

(32). Downing NS; Shah ND; Aminawung JA; Pease AM; Zeitoun JD; Krumholz HM; Ross JS Postmarket safety events among novel therapeutics approved by the US Food and Drug Administration between 2001 and 2010. J. Am. Med. Assoc. (JAMA) 2017, 317 (18), 1854–1863.

(33). Gil C; Ginex T; Maestro I; Nozal V; Barrado-Gil L; Cuesta-Geijo MA; Urquiza J; Ramirez D; Alonso C; Campillo NE; Martinez A COVID-19: Drug targets and potential treatments. J. Med. Chem 2020, 63 (21), 12359–12386. [PubMed: 32511912]

(34). Du L; He Y; Zhou Y; Liu S; Zheng BJ; Jiang S The spike protein of SARS-CoV - a target for vaccine and therapeutic development. Nat. Rev. Microbiol 2009, 7 (3), 226–236. [PubMed: 19198616]

(35). Zhang G; Pomplun S; Loftis AR; Tan X; Loas A; Pentelute BL Investigation of ACE2 N-terminal fragments binding to SARS-CoV-2 Spike RBD. bioRxiv 2020, 2020.03.19.999318.

(36). Otvos L Jr.; Wade JD Current challenges in peptide-based drug discovery. Front. Chem 2014, 2, 62. [PubMed: 25152873]

(37). Henninot A; Collins JC; Nuss JM The current state of peptide drug discovery: Back to the future? J. Med. Chem 2018, 61 (4), 1382–1414. [PubMed: 28737935]

(38). Arkin MR; Wells JA Small-molecule inhibitors of protein-protein interactions: progressing towards the dream. Nat. Rev. Drug Discov 2004, 3 (4), 301–317. [PubMed: 15060526]

(39). Wells JA; McClendon CL Reaching for high-hanging fruit in drug discovery at protein-protein interfaces. Nature 2007, 450 (7172), 1001–1009. [PubMed: 18075579]

(40). Whitty A; Kumaravel G Between a rock and a hard place? Nat. Chem. Biol 2006, 2 (3), 112–118. [PubMed: 16484997]

(41). Buchwald P Small-molecule protein-protein interaction inhibitors: therapeutic potential in light of molecular size, chemical space, and ligand binding efficiency considerations. IUBMB Life 2010, 62 (10), 724–731. [PubMed: 20979208]

(42). Milroy LG; Grossmann TN; Hennig S; Brunsveld L; Ottmann C Modulators of protein-protein interactions. Chem. Rev 2014, 114 (9), 4695–4748. [PubMed: 24735440]

(43). Laraia L; McKenzie G; Spring DR; Venkitaraman AR; Huggins DJ Overcoming chemical, biological, and computational challenges in the development of inhibitors targeting protein-protein interactions. Chem. Biol 2015, 22 (6), 689–703. [PubMed: 26091166]

(44). Song Y; Buchwald P TNF superfamily protein-protein interactions: feasibility of small-molecule modulation. Curr. Drug. Targets 2015, 16, 393–408. [PubMed: 25706111]

(45). Souers AJ; Leverson JD; Boghaert ER; Ackler SL; Catron ND; Chen J; Dayton BD; Ding H; Enschede SH; Fairbrother WJ; Huang DC; Hymowitz SG; Jin S; Khaw SL; Kovar PJ; Lam LT; Lee J; Maecker HL; Marsh KC; Mason KD; Mitten MJ; Nimmer PM; Oleksijew A; Park CH; Park CM; Phillips DC; Roberts AW; Sampath D; Seymour JF; Smith ML; Sullivan GM; Tahir SK; Tse C; Wendt MD; Xiao Y; Xue JC; Zhang H; Humerickhouse RA; Rosenberg SH; Elmore SW ABT-199, a potent and selective BCL-2 inhibitor, achieves antitumor activity while sparing platelets. Nat. Med 2013, 19 (2), 202–208. [PubMed: 23291630]

(46). Gadek TR; Burdick DJ; McDowell RS; Stanley MS; Marsters JC Jr.; Paris KJ; Oare DA; Reynolds ME; Ladner C; Zioncheck KA; Lee WP; Gribling P; Dennis MS; Skelton NJ; Tumas DB; Clark KR; Keating SM; Beresini MH; Tilley JW; Presta LG; Bodary SC Generation of an LFA-1 antagonist by the transfer of the ICAM-1 immunoregulatory epitope to a small molecule. Science 2002, 295 (5557), 1086–1089. [PubMed: 11834839]

(47). Mullard A. Pioneering apoptosis-targeted cancer drug poised for FDA approval. Nat. Rev. Drug Discov 2016, 15 (3), 147–149. [PubMed: 26931080]

(48). Scott DE; Bayly AR; Abell C; Skidmore J Small molecules, big targets: drug discovery faces the protein-protein interaction challenge. Nat. Rev. Drug Discov 2016, 15 (8), 533–550. [PubMed: 27050677]

(49). Tan Q; Zhu Y; Li J; Chen Z; Han GW; Kufareva I; Li T; Ma L; Fenalti G; Li J; Zhang W; Xie X; Yang H; Jiang H; Cherezov V; Liu H; Stevens RC; Zhao Q; Wu B Structure of the CCR5 chemokine receptor-HIV entry inhibitor maraviroc complex. Science 2013, 341 (6152), 1387–1390. [PubMed: 24030490]

(50). Meanwell NA; Krystal MR; Nowicka-Sans B; Langley DR; Conlon DA; Eastgate MD; Grasela DM; Timmins P; Wang T; Kadow JF Inhibitors of HIV-1 attachment: the discovery and development of temsavir and its prodrug fostemsavir. J. Med. Chem 2018, 61 (1), 62–80. [PubMed: 29271653]

(51). Bojadzic D; Buchwald P Toward small-molecule inhibition of protein-protein interactions: General aspects and recent progress in targeting costimulatory and coinhibitory (immune checkpoint) interactions. Curr. Top. Med. Chem 2018, 18 (8), 674–699. [PubMed: 29848279]

(52). Neklesa TK; Winkler JD; Crews CM Targeted protein degradation by PROTACs. Pharmacol. Ther 2017, 174, 138–144. [PubMed: 28223226]

(53). Giannoukakis N; Phillips B; Trucco M Toward a cure for type 1 diabetes mellitus: diabetes-suppressive dendritic cells and beyond. Pediatr. Diabetes 2008, 9 (3 Pt 2), 4–13. [PubMed: 18540865]

(54). Cochrane GM; Horne R; Chanez P Compliance in asthma. Respir. Med1999, 93 (11), 763–769. [PubMed: 10603624]

(55). Moia M; Mantovani LG; Carpenedo M; Scalone L; Monzini MS; Cesana G; Mannucci PM Patient preferences and willingness to pay for different options of anticoagulant therapy. Intern. Emerg. Med 2013, 8 (3), 237–243. [PubMed: 22926743]

(56). Margolles-Clark E; Umland O; Kenyon NS; Ricordi C; Buchwald P Small molecule costimulatory blockade: organic dye inhibitors of the CD40-CD154 interaction. J. Mol. Med 2009, 87 (11), 1133–1143. [PubMed: 19707732]

(57). Bojadzic D; Buchwald P The CD40-targeting KGYY15 peptides do not efficiently block the CD40–CD40L interaction. Diabetologia 2019, 62 (11), 2158–2160. [PubMed: 31501919]

(58). Margolles-Clark E; Jacques-Silva MC; Ganesan L; Umland O; Kenyon NS; Ricordi C; Berggren P-O; Buchwald P Suramin inhibits the CD40–CD154 costimulatory interaction: a possible mechanism for immunosuppressive effects. Biochem. Pharmacol 2009, 77 (7), 1236–1245. [PubMed: 19283894]

(59). Ganesan L; Margolles-Clark E; Song Y; Buchwald P The food colorant erythrosine is a promiscuous protein-protein interaction inhibitor. Biochem. Pharmacol 2011, 81 (6), 810–818. [PubMed: 21219880]

(60). Song Y; Margolles-Clark E; Bayer A; Buchwald P Small-molecule modulators of the OX40–OX40L costimulatory protein–protein interaction. Br. J. Pharmacol 2014, 171 (21), 4955–4969. [PubMed: 24930776]

(61). Chen J; Song Y; Bojadzic D; Tamayo-Garcia A; Landin AM; Blomberg BB; Buchwald P Small-molecule inhibitors of the CD40-CD40L costimulatory protein-protein interaction. J. Med. Chem 2017, 60 (21), 8906–8922. [PubMed: 29024591]

(62). Bojadzic D; Chen J; Alcazar O; Buchwald P Design, synthesis, and evaluation of novel immunomodulatory small molecules targeting the CD40-CD154 costimulatory protein-protein interaction. Molecules 2018, 23 (5), 1153. [PubMed: 29751636]

(63). Bojadzic D; Alcazar O; Buchwald P Methylene blue inhibits the SARS-CoV-2 spike – ACE2 protein-protein interaction – a mechanism that can contribute to its antiviral activity against COVID-19. Front. Pharmacol 2021, 11 (1), 600372. [PubMed: 33519460]

(64). Venkatraj M; Messagie J; Joossens J; Lambeir AM; Haemers A; Van der Veken P; Augustyns K Synthesis and evaluation of non-basic inhibitors of urokinase-type plasminogen activator (uPA). Bioorg. Med. Chem 2012, 20 (4), 1557–1568. [PubMed: 22285569]

(65). Kassack MU; Braun K; Ganso M; Ullmann H; Nickel P; Boing B; Muller G; Lambrecht G Structure-activity relationships of analogues of NF449 confirm NF449 as the most potent and selective known P2X1 receptor antagonist. Eur. J. Med. Chem 2004, 39 (4), 345–357. [PubMed: 15072843]

(66). Buchwald P A single unified model for fitting simple to complex receptor response data. Sci. Rep 2020, 10 (1), 13386. [PubMed: 32770075]

(67). Tan CW; Chia WN; Qin X; Liu P; Chen MI; Tiu C; Hu Z; Chen VC; Young BE; Sia WR; Tan YJ; Foo R; Yi Y; Lye DC; Anderson DE; Wang LF A SARS-CoV-2 surrogate virus neutralization test based on antibody-mediated blockage of ACE2-spike protein-protein interaction. Nat. Biotechnol 2020, 38, 1073–1078. [PubMed: 32704169]

(68). Colson P; Rolain JM; Raoult D Chloroquine for the 2019 novel coronavirus SARS-CoV-2. Int. J. Antimicrob. Agents 2020, 55 (3), 105923. [PubMed: 32070753]

(69). Gordon DE; Jang GM; Bouhaddou M; Xu J; Obernier K; White KM; O'Meara MJ; Rezelj VV; Guo JZ; Swaney DL; Tummino TA; Huettenhain R; Kaake RM; Richards AL; Tutuncuoglu B; Foussard H; Batra J; Haas K; Modak M; Kim M; Haas P; Polacco BJ; Braberg H; Fabius JM; Eckhardt M; Soucheray M; Bennett MJ; Cakir M; McGregor MJ; Li Q; Meyer B; Roesch F; Vallet T; Mac Kain A; Miorin L; Moreno E; Naing ZZC; Zhou Y; Peng S; Shi Y; Zhang Z; Shen W; Kirby IT; Melnyk JE; Chorba JS; Lou K; Dai SA; Barrio-Hernandez I; Memon D; Hernandez-Armenta C; Lyu J; Mathy CJP; Perica T; Pilla KB; Ganesan SJ; Saltzberg DJ; Rakesh R; Liu X; Rosenthal SB; Calviello L; Venkataramanan S; Liboy-Lugo J; Lin Y; Huang XP; Liu Y; Wankowicz SA; Bohn M; Safari M; Ugur FS; Koh C; Savar NS; Tran QD; Shengjuler D; Fletcher SJ; O'Neal MC; Cai Y; Chang JCJ; Broadhurst DJ; Klippsten S; Sharp PP; Wenzell NA; Kuzuoglu D; Wang HY; Trenker R; Young JM; Cavero DA; Hiatt J; Roth TL; Rathore U; Subramanian A; Noack J; Hubert M; Stroud RM; Frankel AD; Rosenberg OS; Verba KA; Agard DA; Ott M; Emerman M; Jura N; von Zastrow M; Verdin E; Ashworth A; Schwartz O; d'Enfert C; Mukherjee S; Jacobson M; Malik HS; Fujimori DG; Ideker T; Craik CS; Floor SN; Fraser JS; Gross JD; Sali A; Roth BL; Ruggero D; Taunton J; Kortemme T; Beltrao P; Vignuzzi M; Garcia-Sastre A; Shokat KM; Shoichet BK; Krogan NJ A SARS-CoV-2 protein interaction map reveals targets for drug repurposing. Nature 2020, 583, 459–468. [PubMed: 32353859]

(70). McKee DL; Sternberg A; Stange U; Laufer S; Naujokat C Candidate drugs against SARS-CoV-2 and COVID-19. Pharmacol. Res 2020,157, 104859. [PubMed: 32360480]

(71). Salgado-Benvindo C; Thaler M; Tas A; Ogando NS; Bredenbeek PJ; Ninaber DK; Wang Y; Hiemstra PS; Snijder EJ; van Hemert MJ Suramin inhibits SARS-CoV-2 infection in cell culture by interfering with early steps of the replication cycle. Antimicrob. Agents Chemother 2020, 64 (8), e00900–20. [PubMed: 32513797]

(72). Clifton J 2nd; Leikin JB Methylene blue. Am. J. Ther 2003, 10 (4), 289–291. [PubMed: 12845393]

(73). Bistas E; Sanghavi D Methylene blue. In StatPearls, Treasure Island; FL, USA, 2020.

(74). Schirmer RH; Adler H; Pickhardt M; Mandelkow E "Lest we forget you--methylene blue…". Neurobiol. Aging 2011, 32 (12), 2325 e7–16.

(75). Dicko A; Roh ME; Diawara H; Mahamar A; Soumare HM; Lanke K; Bradley J; Sanogo K; Kone DT; Diarra K; Keita S; Issiaka D; Traore SF; McCulloch C; Stone WJR; Hwang J; Muller O; Brown JM; Srinivasan V; Drakeley C; Gosling R; Chen I; Bousema T Efficacy and safety of primaquine and methylene blue for prevention of Plasmodium falciparum transmission in Mali: a phase 2, single-blind, randomised controlled trial. Lancet Infect. Dis 2018, 18 (6), 627–639. [PubMed: 29422384]

(76). Cagno V; Medaglia C; Cerny A; Cerny T; Tapparel C; Cerny E Methylene blue has a potent antiviral activity against SARS-CoV-2 in the absence of UV-activation in vitro. bioRxiv 2020, 2020.08.14.251090.

(77). Gendrot M; Andreani J; Duflot I; Boxberger M; Bideau ML; Mosnier J; Jardot P; Fonta I; Rolland C; Bogreau H; Hutter S; La Scola B; Pradines B Methylene blue inhibits the replication of SARS-Cov-2 in vitro. Int. J. Antimicrob. Agents 2020, 106202. [PubMed: 33075512]

(78). Curtis MJ; Alexander S; Cirino G; Docherty JR; George CH; Giembycz MA; Hoyer D; Insel PA; Izzo AA; Ji Y; MacEwan DJ; Sobey CG; Stanford SC; Teixeira MM; Wonnacott S; Ahluwalia A Experimental design and analysis and their reporting II: updated and simplified guidance for authors and peer reviewers. Br. J. Pharmacol 2018, 175 (7), 987–993. [PubMed: 29520785]

(79). Michel MC; Murphy TJ; Motulsky HJ New author guidelines for displaying data and reporting data analysis and statistical methods in experimental biology. J. Pharmacol. Exp. Ther 2020, 372 (1), 136–147. [PubMed: 31884418]

(80). Aldrich C; Bertozzi C; Georg GI; Kiessling L; Lindsley C; Liotta D; Merz KM Jr.; Schepartz A; Wang S The ecstasy and agony of assay interference compounds. J. Med. Chem 2017, 60 (6), 2165–2168. [PubMed: 28244745]

(81). Baell J; Walters MA Chemistry: Chemical con artists foil drug discovery. Nature 2014, 513 (7519), 481–483. [PubMed: 25254460]

(82). Smith CG; O'Donnell JT, The Process of New Drug Discovery and Development. 2nd ed.; Informa Healthcare: New York, 2007; p 657.

(83). Bodor N; Buchwald P Retrometabolic Drug Design and Targeting. 1st ed.; Wiley: Hoboken, NJ, 2012; p 418.

(84). Niesen FH; Berglund H; Vedadi M The use of differential scanning fluorimetry to detect ligand interactions that promote protein stability. Nat. Protoc 2007, 2 (9), 2212–2221. [PubMed: 17853878]

(85). Huynh K; Partch CL Analysis of protein stability and ligand interactions by thermal shift assay. Curr. Protoc. Protein Sci 2015, 79, 28.9.1–14.

(86). Grasberger BL; Lu T; Schubert C; Parks DJ; Carver TE; Koblish HK; Cummings MD; LaFrance LV; Milkiewicz KL; Calvo RR; Maguire D; Lattanze J; Franks CF; Zhao S; Ramachandren K; Bylebyl GR; Zhang M; Manthey CL; Petrella EC; Pantoliano MW; Deckman IC; Spurlino JC; Maroney AC; Tomczuk BE; Molloy CJ; Bone RF Discovery and cocrystal structure of benzodiazepinedione HDM2 antagonists that activate p53 in cells. J. Med. Chem 2005, 48 (4), 909–912. [PubMed: 15715460]

(87). Wössner N; Alhalabi Z; González J; Swyter S; Gan J; Schmidtkunz K; Zhang L; Vaquero A; Ovaa H; Einsle O; Sippl W; Jung M Sirtuin 1 inhibiting thiocyanates (S1th) - a new class of isotype selective inhibitors of NAD(+) dependent lysine deacetylases. Front. Oncol 2020,10, 657. [PubMed: 32426286]

(88). Zhao Y; Ren J; Harlos K; Jones DM; Zeltina A; Bowden TA; Padilla-Parra S; Fry EE; Stuart DI Toremifene interacts with and destabilizes the Ebola virus glycoprotein. Nature 2016, 535 (7610), 169–172. [PubMed: 27362232]

(89). Condor Capcha JM; Lambert G; Dykxhoorn DM; Salerno AG; Hare JM; Whitt MA; Pahwa S; Jayaweera DT; Shehadeh LA Generation of SARS-CoV-2 spike pseudotyped virus for viral entry and neutralization assays: a 1-week protocol. Front. Cardiovasc. Med 2020, 7, 618651. [PubMed: 33521067]

(90). Fletcher S; Hamilton AD Targeting protein-protein interactions by rational design: mimicry of protein surfaces. J. R. Soc. Interface 2006, 3 (7), 215–233. [PubMed: 16849232]

(91). Che Y; Brooks BR; Marshall GR Development of small molecules designed to modulate protein-protein interactions. J. Comput. Aided Mol. Des 2006, 20 (2), 109–130. [PubMed: 16622794]

(92). Hershberger SJ; Lee SG; Chmielewski J Scaffolds for blocking protein-protein interactions. Curr. Top. Med. Chem 2007, 7 (10), 928–942. [PubMed: 17508924]

(93). Reynès C; Host H; Camproux AC; Laconde G; Leroux F; Mazars A; Deprez B; Fahraeus R; Villoutreix BO; Sperandio O Designing focused chemical libraries enriched in protein-protein interaction inhibitors using machine-learning methods. PLoS Comput. Biol 2010, 6 (3), e1000695. [PubMed: 20221258]

(94). Neugebauer A; Hartmann RW; Klein CD Prediction of protein-protein interaction inhibitors by chemoinformatics and machine learning methods. J. Med. Chem 2007, 50 (19), 4665–4668. [PubMed: 17705363]

(95). Sperandio O; Reynes CH; Camproux AC; Villoutreix BO Rationalizing the chemical space of protein-protein interaction inhibitors. Drug Discov. Today 2010, 15 (5-6), 220–229. [PubMed: 19969101]

(96). Levine WG Metabolism of azo dyes: implication for detoxication and activation. Drug Metab. Rev 1991, 23 (3-4), 253–309. [PubMed: 1935573]

(97). Feng J; Cerniglia CE; Chen H Toxicological significance of azo dye metabolism by human intestinal microbiota. Front. Biosci 2012, 4, 568–586.

(98). Roterman I; No KT; Piekarska B; Kaszuba J; Pawlicki R; Rybarska J; Konieczny L Bis azo dyes - studies on the mechanism of complex formation with IgG modulated by heating or antigen binding. J. Physiol. Pharmacol 1993, 44 (3), 213–232. [PubMed: 8241524]

(99). Stopa B; Gorny M; Konieczny L; Piekarska B; Rybarska J; Skowronek M; Roterman I Supramolecular ligands: monomer structure and protein ligation capability. Biochimie 1998, 80 (12), 963–968. [PubMed: 9924974]

(100). McGovern SL; Caselli E; Grigorieff N; Shoichet BK A common mechanism underlying promiscuous inhibitors from virtual and high-throughput screening. J. Med. Chem 2002, 45, 1712–1722. [PubMed: 11931626]

(101). Shoichet BK Screening in a spirit haunted world. Drug Discov. Today 2006, 11 (13-14), 607–615. [PubMed: 16793529]

(102). Feng BY; Shoichet BK A detergent-based assay for the detection of promiscuous inhibitors. Nat. Protoc 2006, 1 (2), 550–553. [PubMed: 17191086]

(103). Capuzzi SJ; Muratov EN; Tropsha A Phantom PAINS: problems with the utility of alerts for Pan-Assay INterference compoundS. J. Chem. Inf. Model 2017, 57 (3), 417–427. [PubMed: 28165734]

(104). Lagorce D; Oliveira N; Miteva MA; Villoutreix BO Pan-assay interference compounds (PAINS) that may not be too painful for chemical biology projects. Drug Discov. Today 2017, 22 (8), 1131–1133. [PubMed: 28676405]

(105). Baell JB; Nissink JWM Seven year itch: pan-assay interference compounds (PAINS) in 2017 - utility and limitations. ACS Chem. Biol 2018, 13 (1), 36–44. [PubMed: 29202222]

(106). Adedeji AO; Severson W; Jonsson C; Singh K; Weiss SR; Sarafianos SG Novel inhibitors of severe acute respiratory syndrome coronavirus entry that act by three distinct mechanisms. J. Virol 2013, 87 (14), 8017–8028. [PubMed: 23678171]

(107). Kao RY; Tsui WH; Lee TS; Tanner JA; Watt RM; Huang JD; Hu L; Chen G; Chen Z; Zhang L; He T; Chan KH; Tse H; To AP; Ng LW; Wong BC; Tsoi HW; Yang D; Ho DD; Yuen KY Identification of novel small-molecule inhibitors of severe acute respiratory syndrome-associated coronavirus by chemical genetics. Chem. Biol 2004, 11 (9), 1293–1299. [PubMed: 15380189]

(108). Severson WE; Shindo N; Sosa M; Fletcher T 3rd; White EL; Ananthan S; Jonsson CB Development and validation of a high-throughput screen for inhibitors of SARS CoV and its application in screening of a 100,000-compound library. J. Biomol. Screen 2007, 12 (1), 33–40. [PubMed: 17200104]

(109). Lundin A; Dijkman R; Bergstrom T; Kann N; Adamiak B; Hannoun C; Kindler E; Jonsdottir HR; Muth D; Kint J; Forlenza M; Muller MA; Drosten C; Thiel V; Trybala E Targeting membrane-bound viral RNA synthesis reveals potent inhibition of diverse coronaviruses including the middle East respiratory syndrome virus. PLoS Pathog. 2014, 10 (5), e1004166. [PubMed: 24874215]

(110). Hanson QM; Wilson KM; Shen M; Itkin Z; Eastman RT; Shinn P; Hall MD Targeting ACE2-RBD interaction as a platform for COVID19 therapeutics: Development and drug repurposing screen of an AlphaLISA proximity assay. ACS Pharmacol. Transl. Sci 2020, 3, 1352–1360. [PubMed: 33330843]

(111). Ou X; Liu Y; Lei X; Li P; Mi D; Ren L; Guo L; Guo R; Chen T; Hu J; Xiang Z; Mu Z; Chen X; Chen J; Hu K; Jin Q; Wang J; Qian Z Characterization of spike glycoprotein of SARS-CoV-2 on virus entry and its immune cross-reactivity with SARS-CoV. Nat. Commun 2020, 11 (1), 1620. [PubMed: 32221306]

(112). Hofmann H; Simmons G; Rennekamp AJ; Chaipan C; Gramberg T; Heck E; Geier M; Wegele A; Marzi A; Bates P; Pohlmann S Highly conserved regions within the spike proteins of human coronaviruses 229E and NL63 determine recognition of their respective cellular receptors. J. Virol 2006, 80 (17), 8639–8652. [PubMed: 16912312]

(113). Tortorici MA; Walls AC; Lang Y; Wang C; Li Z; Koerhuis D; Boons GJ; Bosch BJ; Rey FA; de Groot RJ; Veesler D Structural basis for human coronavirus attachment to sialic acid receptors. Nat. Struct. Mol. Biol 2019, 26 (6), 481–489. [PubMed: 31160783]

(114). Lipinski CA; Lombardo F; Dominy BW; Feeney PJ Experimental and computational approaches to estimate solubility and permeability in drug discovery and development setting. Adv. Drug Deliv. Rev 1997, 23, 3–25.

(115). DeGoey DA; Chen HJ; Cox PB; Wendt MD Beyond the rule of 5: Lessons learned from AbbVie's drugs and compound collection. J. Med. Chem 2017, 61 (7), 2636–2651. [PubMed: 28926247]

(116). Vardhana SA; Wolchok JD The many faces of the anti-COVID immune response. J. Exp. Med 2020, 217 (6), e20200678. [PubMed: 32353870]

(117). Barber DL; Wherry EJ; Masopust D; Zhu B; Allison JP; Sharpe AH; Freeman GJ; Ahmed R Restoring function in exhausted CD8 T cells during chronic viral infection. Nature 2006, 439 (7077), 682–687. [PubMed: 16382236]

(118). Ye Q; Wang B; Mao J The pathogenesis and treatment of the 'cytokine storm' in COVID-19. J. Infect 2020, 80 (6), 607–613. [PubMed: 32283152]

(119). Di Cosimo S; Malfettone A; Perez-Garcia JM; Llombart-Cussac A; Miceli R; Curigliano G; Cortes J Immune checkpoint inhibitors: a physiology-driven approach to the treatment of coronavirus disease 2019. Eur. J. Cancer 2020, 135, 62–65. [PubMed: 32544799]

(120). Petrey AC; Qeadan F; Middleton EA; Pinchuk IV; Campbell RA; Beswick EJ Cytokine release syndrome in COVID-19: Innate immune, vascular, and platelet pathogenic factors differ in severity of disease and sex. J. Leukoc. Biol 2020, ePub.

(121). Icenogle T. COVID-19: infection or autoimmunity. Front. Immunol 2020, 11, 2055. [PubMed: 33042116]

(122). Bastard P; Rosen LB; Zhang Q; Michailidis E; Hoffmann HH; Zhang Y; Dorgham K; Philippot Q; Rosain J; Beziat V; Manry J; Shaw E; Haljasmagi L; Peterson P; Lorenzo L; Bizien L; Trouillet-Assant S; Dobbs K; de Jesus AA; Belot A; Kallaste A; Catherinot E; Tandjaoui-Lambiotte Y; Le Pen J; Kerner G; Bigio B; Seeleuthner Y; Yang R; Bolze A; Spaan AN; Delmonte OM; Abers MS; Aiuti A; Casari G; Lampasona V; Piemonti L; Ciceri F; Bilguvar K; Lifton RP; Vasse M; Smadja DM; Migaud M; Hadjadj J; Terrier B; Duffy D; Quintana-Murci L; van de Beek D; Roussel L; Vinh DC; Tangye SG; Haerynck F; Dalmau D; Martinez-Picado J; Brodin P; Nussenzweig MC; Boisson-Dupuis S; Rodriguez-Gallego C; Vogt G; Mogensen TH; Oler AJ; Gu J; Burbelo PD; Cohen J; Biondi A; Bettini LR; D'Angio M; Bonfanti P; Rossignol P; Mayaux J; Rieux-Laucat F; Husebye ES; Fusco F; Ursini MV; Imberti L; Sottini A; Paghera S; Quiros-Roldan E; Rossi C; Castagnoli R; Montagna D; Licari A; Marseglia GL; Duval X; Ghosn J; Lab H; Group, N.-U. I. R. t. C.; Clinicians, C.; Clinicians, C.-S.; Imagine, C. G.; French, C. C. S. G.; Milieu Interieur, C.; Co, V. C. C.; Amsterdam, U. M. C. C.-B.; Effort, C. H. G.; Tsang JS; Goldbach-Mansky R; Kisand K; Lionakis MS; Puel A; Zhang SY; Holland SM; Gorochov G; Jouanguy E; Rice CM; Cobat A; Notarangelo LD; Abel L; Su HC; Casanova JL Auto-antibodies against type I IFNs in patients with life-threatening COVID-19. Science 2020, 370 (6515), eabd4585. [PubMed: 32972996]

(123). Still WC; Kahn M; Mitra A Rapid chromatographic technique for preparative separations with moderate resolution. J. Org. Chem 1978, 43 (14), 2923–2925.

(124). Schneider CA; Rasband WS; Eliceiri KW NIH Image to ImageJ: 25 years of image analysis. Nat. Methods 2012, 9 (7), 671–675. [PubMed: 22930834]

(125). Adachi Y; Nakagawa H; Matsuo K; Suzuki T; Miyata N Photoactivatable HNO-releasing compounds using the retro-Diels-Alder reaction. Chem. Commun 2008, (41), 5149–5151.

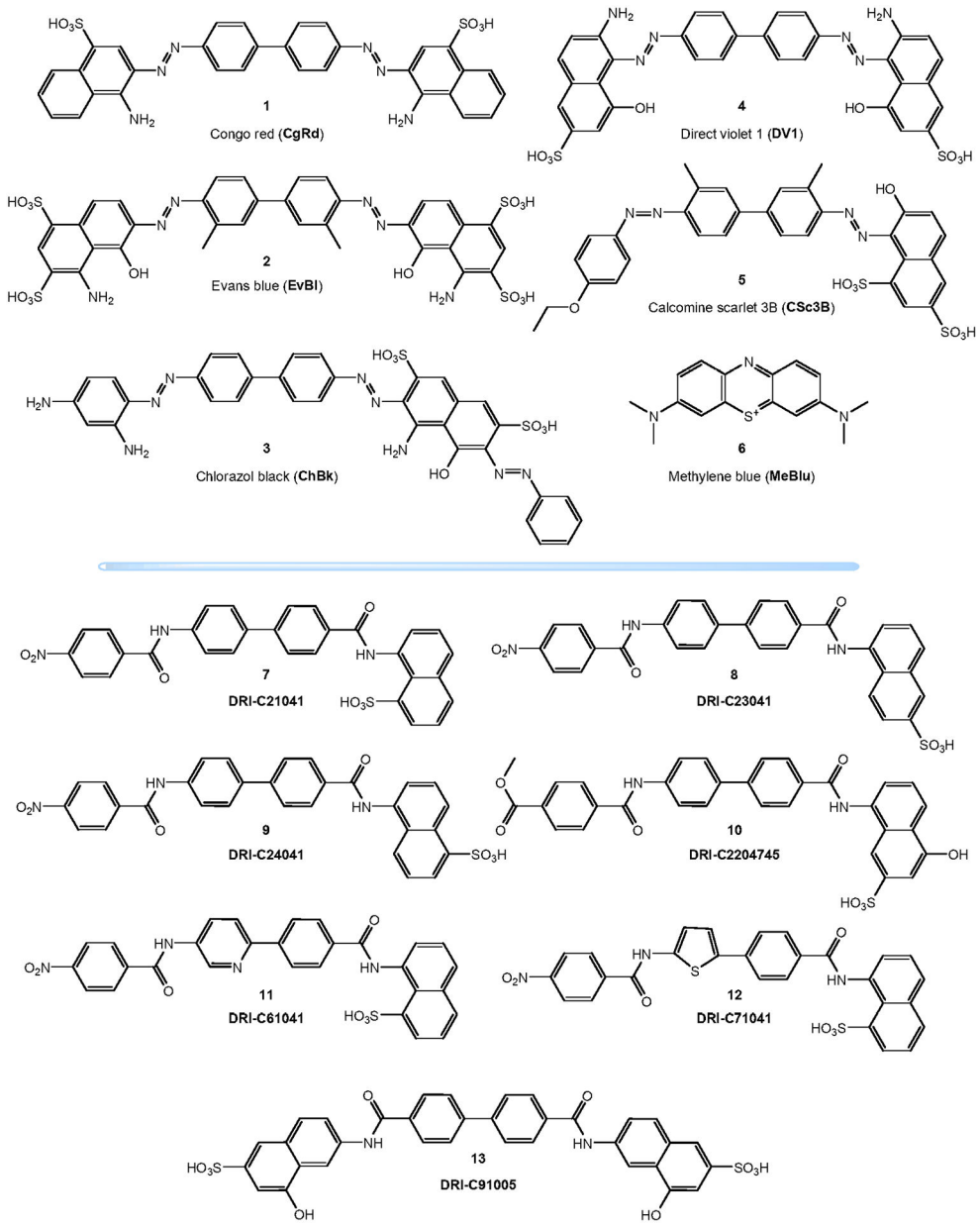

Figure 1. Compounds of the present study.

Chemical structures of the organic dye (**1-6**) and non-dye DRI-C compounds (**7-13**) used in the present study.

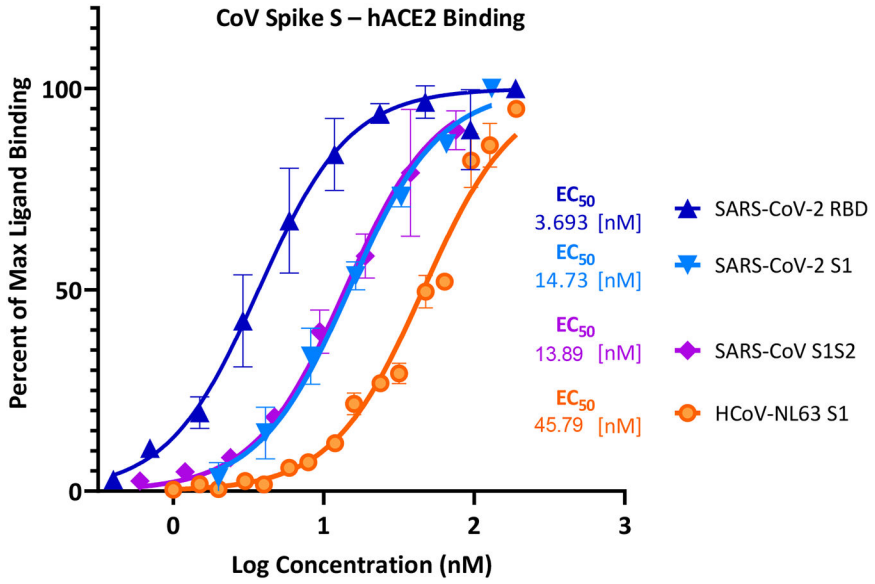

Figure 2. Concentration-response curves for binding of CoV spike protein domains to human ACE2 in cell-free ELISA-type assays.

Binding curves and corresponding EC_{50}s are shown for SARS-CoV-2 (RBD and S1), SARS-CoV (S1&S2), and HCoV-NL63 (S1). They were obtained using Fc-conjugated hACE2 coated on the plate and His-tagged S1, S1S2, or RBD added in increasing amounts as shown with the amount bound detected using an anti-His–HRP conjugate (mean ± SD for two experiments in duplicates).

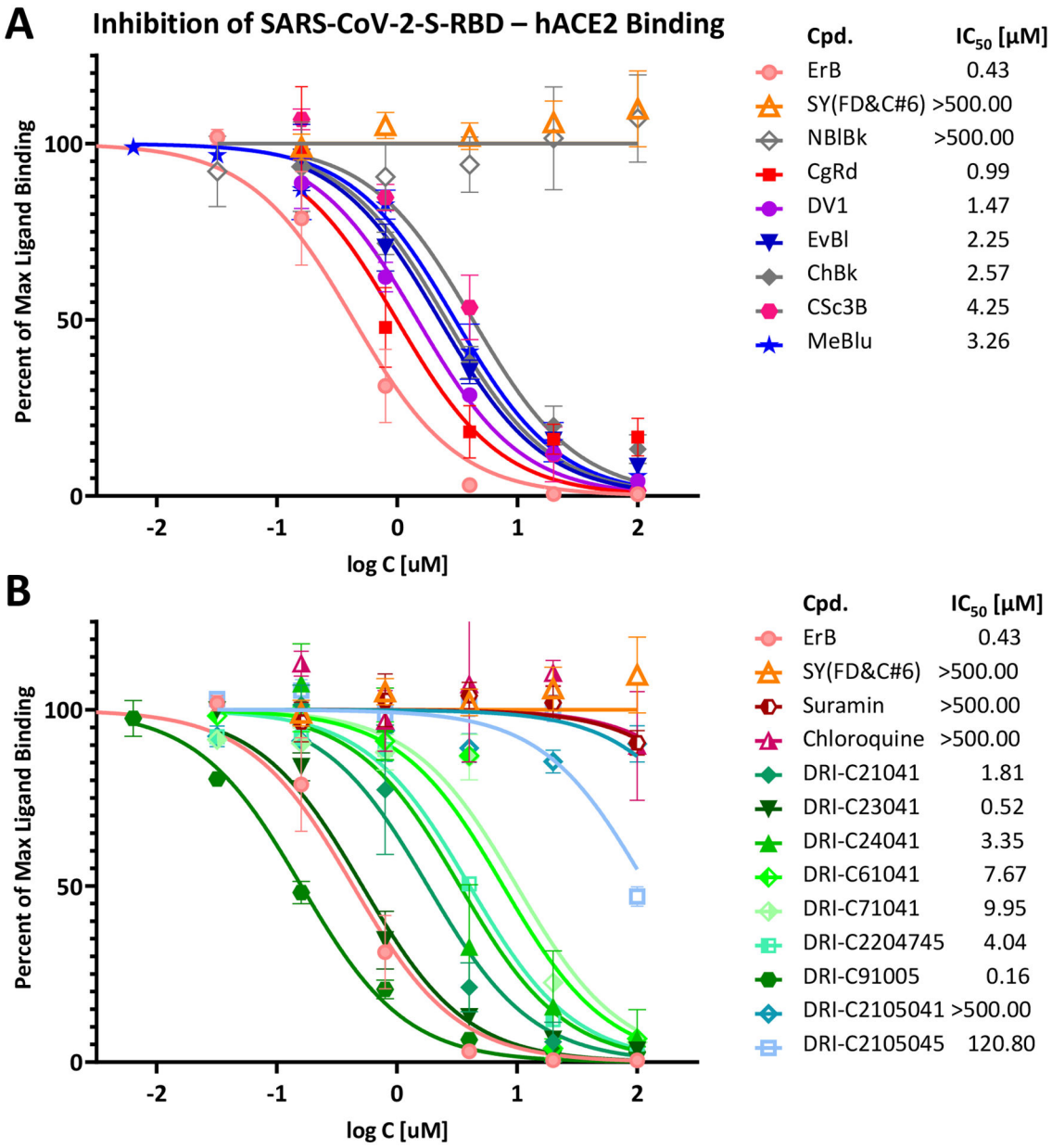

Figure 3. Concentration-dependent inhibition of SARS-CoV-2-S-RBD binding to ACE2 by compounds of the present study.

Concentration-response curves obtained for the inhibition of the PPI between SARS-CoV-2-RBD (His-tagged, 0.5 μg/mL) and hACE2 (Fc-conjugated, 1 μg/mL) in cell-free ELISA-type assay with dye (**A**) and non-dye (**B**) compounds tested. The promiscuous PPI inhibitor erythrosine B (ErB) and the food colorant FD&C yellow no. 6 (sunset yellow, SY) were included as a positive and negative controls, respectively. Data are mean ± SD from two experiments in duplicates and were fitted with standard sigmoid curves for IC_{50} determination. Estimated IC_{50}s are shown in the legend indicating that while suramin and chloroquine were completely inactive (IC_{50} > 500 μM), several of our in-house compounds including organic dyes (CgRd, DV1, and others) as well as proprietary DRI-C

compounds (e.g., DRI-C23041, DRI-CC91005) showed promising activity, some even at sub-micromolar levels (IC_{50} < 1 μM).

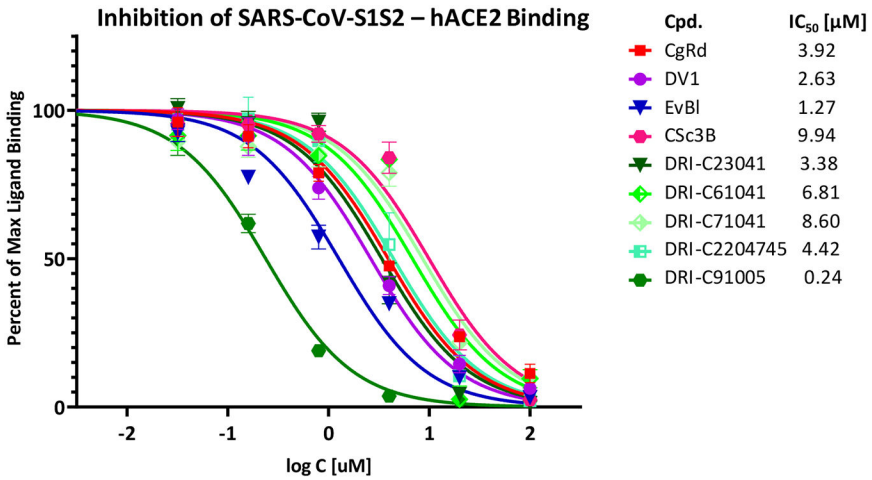

Figure 4. Concentration-dependent inhibition of SARS-CoV-S1S2 binding to ACE2 by representative compounds of the present study.

Concentration-response curves obtained for the inhibition of the PPI between SARS-CoV-S1S2 (His-tagged, 1 μg/mL) and hACE2 (Fc-conjugated, 1 μg/mL) in cell-free ELISA-type assay by selected representative dye and non-dye compounds. Data and fit as before (Figure 3). Most compounds including several DRI-C compounds show similar activity against SARS-CoV (i.e., SARS-CoV-1) as against SARS-CoV-2 raising the possibility of broad-spectrum activity.

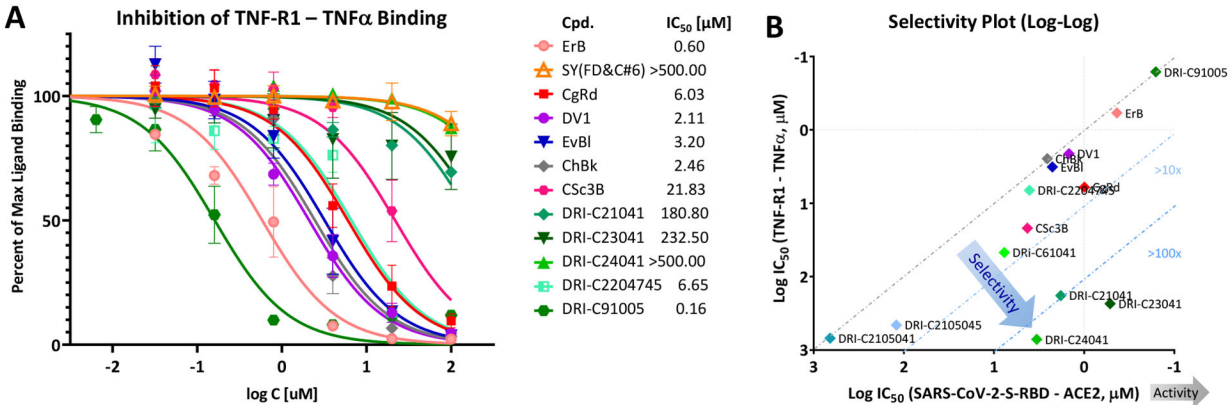

Figure 5. Concentration-dependent inhibition of TNF-R1–TNFα by compounds of the present study and corresponding selectivity plot.

(**A**) Concentration-response curves obtained for the inhibition of this important TNF superfamily PPI in similar cell-free ELISA-type assay as used for the CoV-S–ACE2 PPIs to assess selectivity. Data and fit as before (Figure 3). As the IC_{50} values indicate, DRI-C compounds showed more than 100-fold selectivity in inhibiting the CoV-S PPI vs the TNF PPI. (**B**) Selectivity plot comparing inhibitory activity (as quantified by log IC_{50}) against the TNF-R1–TNF-α interaction with that against the desired PPI target (SARS-CoV-2-S-RBD–hACE2). Active and selective compounds are clustered in the lower right corner as highlighted by the trend-indicating arrows.

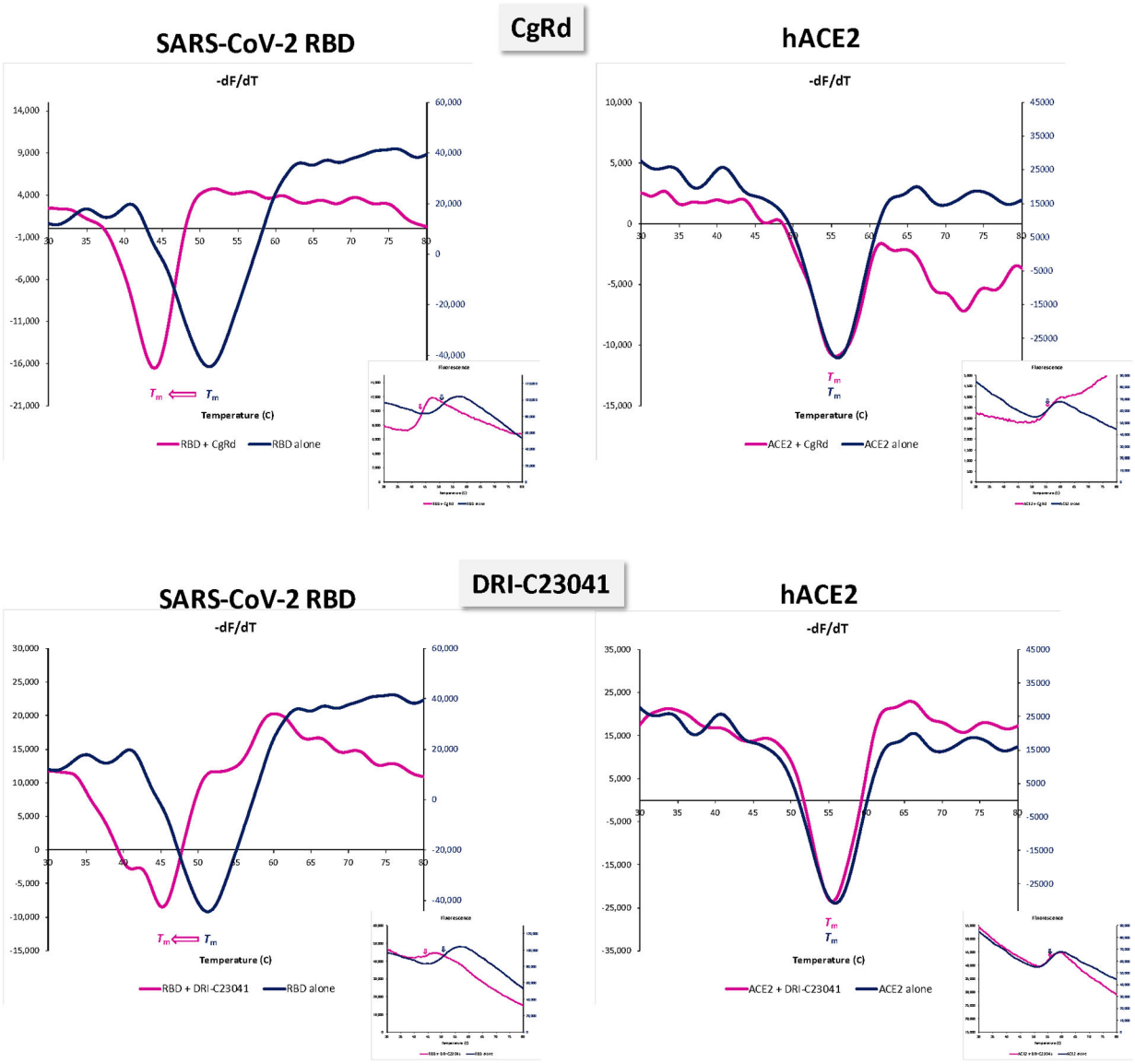

Figure 6. Identification of the binding partner by protein thermal shift.

Differential scanning fluorimetry assay indicating SARS-CoV-2 RBD and not ACE2 as the binding partner of the present SMI compounds. The presence of Congo red (top) or DRI-C23041 (bottom) at 10 μM caused clear shifts in the melting temperature of the protein for RBD as indicated by the derivatives d*F*/d*T* (left; purple vs. blue line), but not for hACE2 (right) (smaller insets are normalized fluorescence *F* data).

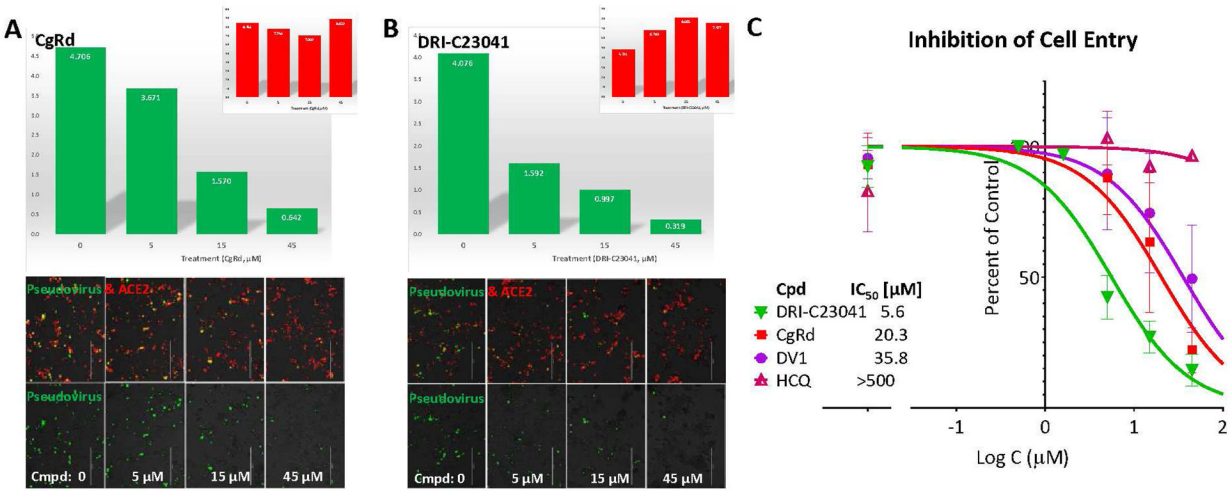

Figure 7. Concentration-dependent inhibition of SARS-CoV-2 pseudovirus entry (BacMam) into hACE2 expressing host cells by selected compounds.

Quantification of entry of pseudoviruses bearing the SARS-CoV-2 S protein (plus green fluorescent protein reporters; BacMam-based) in ACE2 (plus red fluorescence) expressing host cells (HEK293T). Representative images (bottom row) and their quantification for pseudovirus (green) and ACE2 expression (red) using ImageJ (top row) are shown from one experiment for CgRd and DRI-C23041 in **A** and **B**, respectively; average data from three experiments fitted with typical concentration-response curves are shown in **C**. The amount of green present is proportional with the number of infected cells as green fluorescence is expressed only in pseudovirus infected cells, while amount of red is proportional with the number of ACE2-expressing cells. The organic dye CgRd (**A**), but especially DRI-C23041 (**B**) showed concentration-dependent inhibition with activities corresponding to low micromolar IC_{50} values, whereas hydroxychloroquine (HCQ) showed no effect (**C**).

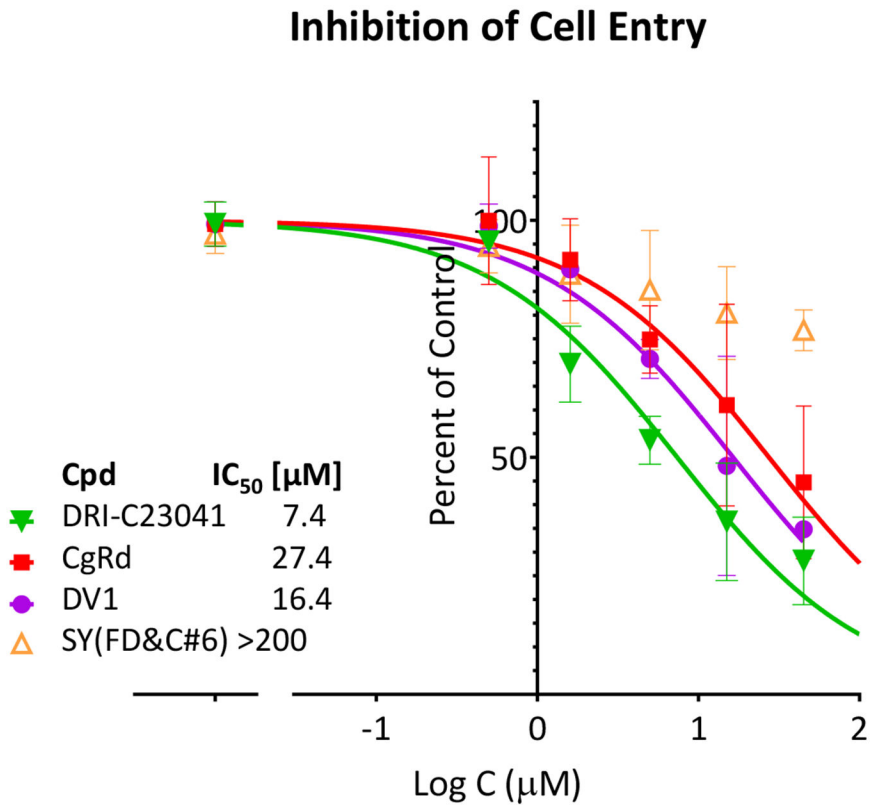

Figure 8. Concentration-dependent inhibition of SARS-CoV-2 pseudovirus (VSV-ΔG) entry into hACE2/Furin expressing host cells by selected compounds.

Entry of VSV-ΔG pseudoviruses bearing the SARS-CoV-2 S protein (plus GFP reporters) in ACE2/Furin overexpressing host cells (Vero-E6) was quantified via GFP fluorescence in a live imaging system (Incucyte). CgRd and DRI-C23041 showed concentration-dependent inhibition with IC_{50} values consistent with the previous assay (Figure 7), whereas the negative control sunset yellow (SY FD&C #6) showed no significant effect.